DSN
24

RADC-TR-65-142
Final Report

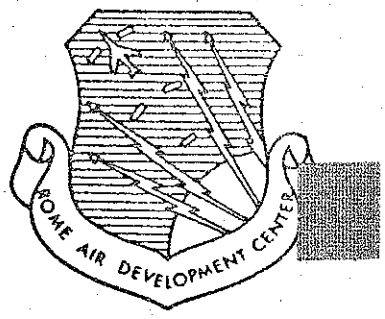

NANOSECOND PULSE BREAKDOWN IN GASES

P. Felsenthal
J. M. Proud

TECHNICAL REPORT NO. RADC-TR- 65-142
June 1965

20-P

Techniques Branch
Rome Air Development Center
Research and Technology Division
Air Force Systems Command
Griffiss Air Force Base, New York

NANOSECOND PULSE BREAKDOWN IN GASES

P. Felsenthal
J. M. Proud

AFLC, GAFB, N.Y. 4 Aug 65-138

FOREWORD

This final technical report was prepared under contract AF30(602)-2779 by Space Sciences, Inc., 301 Bear Hill Road, Waltham, Mass.

The work was performed under Project 4506, Task 450603, and was monitored by Mr. R. Blackall, RADC Project Engineer.

This technical report has been reviewed and is approved.

Approved: RONALD C. BLACKALL
AlC, USAF
Project Engineer

Approved: THOMAS S. BOND, JR.
Colonel, USAF
Chief, Surveillance
and Control Division

FOR THE COMMANDER:

IRVING S. GABELMAN
Chief, Advanced Studies Group

ABSTRACT

It is shown analytically that under certain conditions pulsed dc and pulsed microwave breakdown are directly comparable. A pulsed dc experimental system to measure breakdown over a wide range of applied voltage, gas pressure and gap distance has been used to measure formative time in the different gases. For those gases where sufficient basic data are available comparison of theoretical and experimental results show good agreement. Breakdown measurements in air have been used to calculate breakdown field strengths as a function of altitude and frequency for pulse lengths of 1 to 100 nanoseconds.

TABLE OF CONTENTS

TABLE OF FIGURES

TABLE OF TABLES

EVALUATION

RADC has been working in the nanosecond pulse field for the past three years with an ultimate goal of utilizing high power nanosecond pulses to establish techniques for long range radar with superior range resolution. Because of the extreme peak powers, the first logical step was the investigation of gaseous breakdown under short pulse conditions. The content of this report represents the end result of 2 1/2 years of effort at Space Sciences in which nanosecond video pulse breakdown has been theoretically and experimentally investigated. While the experimental work utilized video pulses, the data is applicable to the microwave case by means of the diffusion theory. The latter was checked by comparison with the work of Microwave Associates described below in the last paragraph.

The air breakdown data, with suitable corrections to the microwave pulse case, has been used to generate a series of curves describing atmospheric breakdown as a function of altitude, pulse length, frequency and field strength. These curves all assume some ionization present for initiating breakdown. Complementary work being done at Braddock, Dunn and McDonald[1] indicates that there will be a near certainty of a propagating pulse encountering at least one free electron in the atmosphere. RADC in-the-house investigators[2] have calculated that for a given frequency, beam width, power and pulse length, there is a fairly well defined volume of atmosphere in which breakdown is possible dependent on the availability of an initiating electron. The probability of encountering an electron in this volume varies from 0 to 30%, depending on several factors. A report treating this and also containing other pertinent nanosecond information is currently in preparation.

Other contractors investigating nanosecond pulse breakdown are Braddock, Dunn and McDonald, El Paso, Texas, and Microwave Associates, Burlington, Mass. Braddock, Dunn and McDonald is currently investigating conditions which lead to breakdown initiation, surface conditioning, and high power nanosecond pulse propagation through the atmosphere (Contract AF30(602)-2781, "Nanosecond Pulse Breakdown Study"). Microwave Associates has investigated breakdown at microwave X-Band frequencies with nanosecond pulses (Contract AF30(602)-2782, "Nanosecond R.F. Pulse Breakdown Study").

Ronald C. Blackall

RONALD C. BLACKALL
A1C, USAF
Project Engineer

1 Braddock, Dunn and McDonald, El Paso, Texas, Contract AF30 (602)-2781, report RADC-TR-64-584.

2 W. Quinn, F. Welker, R. Blackall

1. Introduction

This report summarizes the results of a program to investigate dc nanosecond breakdown in various gases including air, N_2, O_2, He, A, SF_6, Freon 12, Freon 114, Freon C318. Emphasis in this study has been placed on establishing a firm theoretical linking of dc video breakdown and pulsed microwave breakdown and on obtaining accurate breakdown data in a variety of gases.

The comparison of breakdown measurements and theoretically derived breakdown curves show that the diffusion theory employed to describe microwave breakdown is also a proper description of the formative period of dc breakdown. Hence the data given in this report are directly applicable (through the formalism of diffusion theory) to the problem of super high power nanosecond pulse microwave breakdown. Thus we have included calculations giving high power, short pulse breakdown parameters for various frequencies in air for altitudes of 0 to 100,000 feet.

The report is divided into three sections. The first gives the theoretical background and foundation for a description of dc nanosecond breakdown. The second section describes the experiment and gives full results for the nine different gases. The third section applies the results obtained in air to the problem of high power, short pulse electromagnetic wave propagation through the atmosphere.

2. Theory

2.1. Background

The electrical breakdown of a gas is, in general, characterized by the net build-up of ionization from processes within the gas and from a host of secondary processes at walls and electrodes of the discharge vessel. Under certain conditions it has been possible to investigate breakdown with cw microwave techniques[1,2,3] where the electron generation and loss mechanisms are confined to the gas alone. The applicable diffusion theory then accounts for the balance between impact ionization as the generation process and attachment and diffusion as the loss processes. The validity of the diffusion theory [3] is subject to requirements on field uniformity, electron mean free path and the amplitude of electron oscillation in the alternating field. The same theory has been applied successfully to the investigation of the formative time for breakdown under pulsed microwave conditions[4]. An additional simplification can be achieved in this case since it is possible to design experiments in which the diffusion loss of electrons is negligible.

The research described in this report was undertaken with the premise that the restriction of breakdown processes to those taking place in the gas could also be achieved under pulsed dc breakdown conditions. Under these conditions the formative processes of breakdown can be described within the same theoretical framework as employed in microwave breakdown and the experimental results for the two types of breakdown are unified. Moreover, the pulsed dc methods materially extend the range of breakdown parameters beyond that previously studied, especially where high electric field values are required for breakdown.

In taking this approach, we have departed somewhat from conventional descriptions of the formative processes in dc breakdown. In the investigation of formative lag in overvolted atmospheric gaps, Fletcher [5] analysed his results in terms of a streamer model of the breakdown process. Following a suggestion of Raether, [6] Fletcher computed the formative time as the time for

an initial electron avalanche to build up a space charge field comparable to the applied field. Dickey [7] later showed that a simpler calculation of the breakdown times reported by Fletcher could be formulated by discarding the streamer model and by estimating the growth rate of ionization and subsequent charge separation in the undistorted applied field. This approach not only yields reasonable agreement for the formative time, but also explains the observed pulse shapes just following breakdown. In the theory employed in our investigation we also consider the field to be undistorted by space charge during the development of breakdown just as in the microwave breakdown theory [2]. The limits of the theory for effectively electrodeless dc pulse breakdown are then derived in a manner which is closely analogous to the development of validity limits for the diffusion theory of microwave breakdown. The limits so defined are then at once the limits for validity of theory and the limits within which experimental results using dc pulse technique are comparable to those obtained by microwave methods.

2.2. Theoretical Model

The model on which the theory is based is one in which a voltage pulse is instantaneously applied to a gas contained between effectively infinite parallel plate electrodes. It is assumed that the statistical lag component of the breakdown lag is eliminated by insuring that a supply of initial electrons exists at the instant the overvoltage is applied. The formative lag time is then the measured characteristic time for build-up of ionization in the gap space. The appropriate form of the electron continuity equation which relates the net rate of change of electron density to the generation and loss mechanisms is then

$$\frac{\partial n}{\partial t} = \nu_i n - \nu_a n - \nabla \cdot \Gamma \qquad (1)$$

where n is the electron density, ν_i is the ionization frequency, ν_a is the attachment frequency and Γ is the particle flow. In general, Γ will consist of

diffusion and mobility components. However, to achieve effectively electrodeless conditions we must establish experimental design requirements such that the electron current does not lead to wall or electrode interactions within the time of interest. This is equivalent to the requirement that the term $\nabla \cdot \Gamma$ be neglected in Equation (1). Since the mobility term will dominate in the pulsed dc case, the condition which permits the neglect of this term is similar to that imposed by the oscillation amplitude limit in the case of microwave breakdown theory.

2.3. Validity Limits

To evaluate this and other limits of the theory as applied to pulsed dc breakdown, it is useful to choose the following set of variables

$$P\tau \ , \ P\Lambda \ , \ E/P$$

where P is the gas pressure, τ is the formative time, E is the applied field and Λ is the characteristic diffusion length. For infinite parallel plate geometry $\Lambda = d/\pi$ where d is the plate separation. The limits which must be imposed may now be conveniently presented in the $P\Lambda$ - $P\tau$ plane. The Mobility Amplitude Limit may be expressed by equating the plate separation to the electron drift distance during the formative period. In terms of the above variables we obtain

$$P\Lambda = \pi^{-1} k \, E/P \cdot P\tau \qquad (2)$$

where k is the product of electron mobility and the pressure. The limit line is derived empirically from the formative time data which provide the values of E/P and $P\tau$.

If the formative time is short compared to the time of propagation of the voltage pulse across the gap, uniform field conditions will not exist. Hence, the Uniform Field Limit is expressed by

$$P\Lambda = \frac{c}{\pi} \cdot P\tau \qquad (3)$$

where c is the wave velocity in the gap. As will be seen by examples below

the limit lines represented by Equations (2) and (3) are the important boundaries for validity of the theory. However, two additional considerations are noteworthy concerning the mean free path and the collision frequency. The Mean Free Path Limit arises when the mean free path is comparable to the gap separation, or

$$P\lambda = 1/P_c \tag{4}$$

where P_c is the probability of collision. Assuming a constant value for P_c, the limit line is a horizontal line in the lower portion of the $P\lambda$ - $P\tau$ plane.

The situation in which a rapid build-up of ionization occurs by impact ionization clearly requires many collisions during the pulse length, and one does not expect to observe breakdown by this process in time scales which are comparable to the mean collision time. Therefore, we shall always be concerned with conditions for which many collisions occur within the formative time. In this sense, it is proper to consider a Collision Frequency Limit defined by

$$P\tau = P/\nu_c \tag{5}$$

where ν_c is the collision frequency.

The four limit lines are illustrated for air breakdown in Figure (1). The portion of the plane bounded by the Uniform Field Limit on the left and the Mobility Amplitude Limit on the right is then the region within which the breakdown mechanisms are governed by gaseous processes in uniform applied fields. In reaility, of course, the boundaries indicated cannot be construed as precise since certain arbitrary choices of parameters have been exercised in Equations (2) through (5) and electron distributions have been ignored in favor of dealing with average electron behavior.

The breakdown parameters employed in the experiments for air reported below were located within a zone removed from each limit line. This zone is indicated by the large shaded area in Figure (1). In the other gases studied, where mobility data was available, similar zones were established in the $P\tau$ -

$P\lambda$ plane. The range of parameters associated with Fletcher's measurements in atmospheric gaps is also shown in the figure. The location of his breakdown parameters is near the Mobility Amplitude Limit line suggesting that electrode processes played a role in the formative lag times which he measured.

2.4. Breakdown Equation

With the neglect of the drift loss term, Equation (1) integrates to

$$\ln \frac{n_b}{n_o} = (\nu_i - \nu_a) \cdot \tau \tag{6}$$

where n_b/n_o is the ratio of the breakdown electron density to the initial density. The ionization and attachment frequency may be written in terms of the Townsend first ionization coefficient α, the attachment coefficient β and the drift velocity $k\,E/P$ to yield

$$P\tau = \frac{\ln n_b/n_o}{k\,E/P\,(\alpha/P - \beta/P)} \tag{7}$$

Use has been made of this expression with available data for k, α/P and β/P to formulate the theoretical curves of E/P versus $P\tau$ for each of the gases studied. The extent of the available data and the extrapolation techniques are discussed in Appendix I.

Equation (7) is plotted for air in Figure 2 and compared with Fletcher's data, with results obtained by Gould and Roberts and with the average experimental curve obtained in this investigation. The generally good agreement between theory and experiment and the fact that the microwave and dc pulse data are in accord with the same theory (see Section 4.1) appear to support the approach taken above.

3. Experiment

3.1. Results and Parameter Summaries

Breakdown measurements have been performed in a number of gases. The apparatus and technique are described in Sections 3.2 and 3.3 below. Basically the apparatus applies a short rise-time pulse to a test gap and allows the direct measurement of the sum of the formative time and statistical time. Because the gap distance, gas pressure and pulse voltage are known and the statistical time may be removed from the measurement, it is possible to measure E/P and $P\tau$ for various gases over a wide range of parameters. Table I gives a summary of the laboratory variables used in the measurement of each gas as well as the nominal purity of each gas. The results of the investigation are illustrated in Figures 3 through 20 for the nine gases. These figures include the breakdown data with curves of the average measured results and the theoretically predicted curves where possible. The latter curves were derived from Equation (7) by the methods described in Appendix I. The second figure for each gas is a plot of the breakdown parameters in relation to the validity limits. Figure (21) summarizes the breakdown results for all nine gases.

3.1.1. Air Results

The results in air are particularly interesting both because they may be compared with previous work and because they are of great practical interest. A detailed plot of our experimental results in air along with the air theoretical formative time curve is shown in Figure (3). The experimental curve is drawn through the average of the experimental points. Experimental breakdown data have been obtained for much higher E/P values then can be treated by the theory due to a lack of fundamental data at $E/P > 10^3$ volts/cm-mm Hg. The data above this value are suggestive of an asymptotic approach to a minimum value of $P\tau$. It is plausible that this is brought about by an approach to conditions such that the collision frequency and ionization frequency are equal. Figure (4) illustrates the diffusion theory limits discussed in Section 2.3 and their relationship to our experimental points. The Mobility Amplitude Limit Line analytic

expression was derived from the drift velocity expression as described in Appendix I by an iterative procedure which employs averaged breakdown results.

3.1.2. Nitrogen, Oxygen, Argon and Helium Results

The results for nitrogen, oxygen and argon were obtained in a manner similar to that for air. Commercial quality gases were used in the experiments. Their purity is listed in Table I. The results of breakdown measurements in these gases are shown in Figures (5 - 10).

Two sets of ionization coefficient data for helium are available (see Appendix I). Predictions based on these two sets of ionization data are shown in Figure (11) along with the results of the present measurements. Agreement at the larger values of $P\tau$ is closest to predictions based on data of [19] while at smaller values of $P\tau$ agreement is best with theory based on [25] information. It is conjectured that this situation may be traced to similarities in gas purity between the referenced work and the present breakdown experiments. The breakdown measurements were carried out with impurities ranging from 1 part in 10^3 at values of $E/P > 500$ volts/cm-mm Hg to 1 part in 10^5 at lower values. The experimental variation in purity was due to the experimental conditions of vacuum and continuous flow.

One interesting aspect of helium breakdown that has appeared in the experimental results is a reduction of breakdown pulse current for low pressures. For pressures of 1 mm Hg the equivalent gap impedance after the gap has broken down is many hundreds of ohms as against a fraction of an ohm under normal circumstances.

3.1.3. Insulating Gas Results

Results have been obtained in four insulating gases. For two of the gases, Freon 114 ($CC1F_2$ - $CC1F_2$) and Freon C318 (C_4F_8 cyclic) there exist no experimental data on any of the appropriate gas discharge parameters. Hence for these gases we present only the experimental points and an average curve of the experimental points (Figures 17 - 20).

For Freon 12 (CCl_2F_2) and SF_6 there exists a limited amount of gas discharge data, specifically data on α/P and β/P (see Appendix I). By an iterative process we have used our breakdown data Figures (13 - 16) to determine an electron drift velocity expression in these gases and have formulated an estimate of α/P over a range of E/P where no previous results exist (see Appendix II).

3.1.4. Breakdown in Moist Air and Ozone

In order to justify extension of our air breakdown data to the atmosphere, breakdown measurements in air of varying degrees of humidity were performed. Tests were made in dry air, 45.3% and 100% relative humidity air as well as in air containing a large amount of water in aerosol suspension. These tests performed in gaps of 0.18 and 0.31 cm at room pressure showed no effect on formative time due to moisture content.

Tests were also performed on the effect of ozone enriched air on formative times. The results shown in Figure (22) show a slight increase in formative times with increasing ozone concentration but no significant change exists from the pure air measurements. These results are particularity applicable to waveguide and radome structures where the ozone concentration has a chance to build up to high levels. It should be noted that the maximum concentration shown in Figure (22) is 10^4 times greater than the maximum allowable for nontoxic effects on humans.

3.2. Apparatus

The experimental apparatus is capable of measuring breakdown times in the regime described by the above theory of Section 2. The apparatus allows a wide range of the parameter E/P to be examined, while maintaining time resolution of 0.3 nanoseconds. Gap distances and pressures may also be varied over a wide span of values.

Two functional capabilities underscore the apparatus design throughout. First, consideration had to be given to the high voltage capability of the overall pulse circuit, which must be capable of passing and switching nanosecond pulses

of many kilovolts amplitude. Secondly, because of the short pulse duration, the frequency spectrum of the pulses generated extends from dc to the gigacycle range. Therefore, the entire apparatus is designed as a transmission line system with a frequency response spanning this spectrum.

The electrical system is similar to that developed by Fletcher [8]. It provides for the generation of pulses with rise times of 0.29 to 1.0 ns with amplitudes of 4 to 30 kilovolts. It also provides an attenuated sample of the pulse for measurement of breakdown times, appropriate triggers and a source of ultraviolet light for illumination of the test gap. A schematic of the system is shown in Figure (23). The main pulse generator is a high pressure coaxial three ball gap used to discharge a 60 ns length of RG-17. The two outer balls may be moved axially relative to the fixed center ball. The gap is of tapered 52 ohm coaxial construction with a small pulse shaping condensor incorporated in the charging line side of the gap. Gas pressure and ball gap distance are adjusted to give proper operation at various cable charge voltages. Nitrogen or argon with pressures from 80 to 200 psig is used as the insulating gas.

The coaxial current viewing resistor is 0.212 ohm (supplied by T & M Research Products, Albuquerque, New Mexico). The resistor output is passed through a 4 gc bandwidth coaxial pad of 6, 10 or 13 db and then to a 3 db power divider and a matching transformer for the 125 ohm oscilloscope deflection system. The other output of the power divider is used to trigger the oscilloscope. A Tektronix 519 oscilloscope with a deflection sensitivity of 9.8 v/cm and rise time of 0.29 nanoseconds is used to view the signals. With the aid of ASA 10,000 Polaroid film and an image reduction of 2:1, single trace photographs at 2 nanoseconds/cm may be obtained.

In addition to the current viewing resistor, the transmission line connecting the pulse generator and the test gap contains a 10 meg ohm resistor between the center and outer conductors to dissipate any net charge left on this portion of the system after the high voltage pulse has been applied to the test gap. A 50 ohm termination on the other side of the test gap provides a proper load for pulses transmitted through the gap when breakdown occurs.

The system trigger and ultraviolet illumination for the cathode are provided by the charged length of RG-8. A low voltage pulse is used to start the discharge of a ball-to-plane-to-point air gap. A first surface, 2.5 cm focal length mirror is used behind the plane-to-point discharge to increase the light output. The high voltage pulse from this discharge is used to trigger the pulse generator.

Two different test gaps have been used in the measurements reported here. Both gaps are basically the same tapered, 52 ohm coaxial construction. Polystyrene was used as the insulating material because of its low and uniform dissipation factor over the range of frequencies contained in the pulse. Both gaps have quartz windows for the admission of ultraviolet light to the cathode surface, ports for the admission of the test gases and pumping ports. Polished aluminum electrodes with Rogowski contours [9] are used to provide uniform field conditions. The small gap is approximately 7.6 cm inside diameter with electrodes 3.5 cm diameter. The gap distance is adjustable by means of a 20 turns per inch thread. Gap distance of 0.051 to 0.5 centimeters are used. The large gap, Figure (24), is approximately 20.2 cm inside diameter with electrodes of 8.0 cm diameter. Fixed spacers are used to provide gap distances of 2.0, 4.0 and 6.0 centimeters. The maximum error in setting the gap distance is estimated to be less than 5%. A two stage mechanical pump with a zeolite trap is used to evacuate the test gap. Ultimate pressure of both gaps as measured on an Alphatron gauge is in the range of 1 to 2 x 10^{-3} mm Hg. During measurements the test gas is admitted through a variable leak, and the pumping speed reduced by a throttling valve. Thus a small flow of gas through the test gap is insured at all times. A standard mercury manometer is used as a check on the Alphatron gauge. Pressure measurements in the gap have an estimated accuracy of $\pm$ 2%.

The 20 kilovolt supply for the RG-8 line is fixed in output voltage so that adjustment of the air spark gap is unnecessary. Two separate supplies are used for charging the RG-17 line. A 0 to 13 kilovolt supply is used for low voltages and a 0 to 60 kilovolt supply for voltages from 16 to 30 kilovolts. Both supplies are 1% regulated and may be set to a given voltage with an

average accuracy of $\pm$ 2%. However, because of aging of internal components in the supplies, the overall voltage accuracy is about $\pm$ 5%. When the RG-17 pulse cable is charged to a voltage V_o and discharged, the amplitude of the traveling wave is $V_o/2$. When the pulse reaches the test gap it is reflected back into the RG-17 coupling cable until such time as the test gap begins to conduct appreciable current. During the time that the traveling pulse is being reflected from the test gap electrode the voltage across the gap is V_o. Measurement of the traveling pulse amplitude seen through the current viewing resistor show it to be Vo/2 within 1%. Hence, we have assumed that the voltage to which the pulse cable is charged is the voltage applied to the test gap and that losses in the high pressure pulse generator are negligible. Rise time of the pulse depends on the particular voltage, the gas pressure in the pulse generator and the electrode distance. Rise times of 0.25 to 1.0 nanoseconds are observed. Ringing and overshoot are normally less than 10% of the average pulse amplitude. As may be seen the typical ringing frequency is of the order of a few hundred megacycles. The exact amount of ringing not only varies with the voltage and gap setting but fluctuates slightly on a pulse to pulse basis. The rise time varies similarly.

The measurements of breakdown in ozone and humid air were performed with modified gas handling equipment. All measurements were performed at atmospheric pressure so that it was possible to use a closed recirculating system for handling the breakdown gas. For the ozone measurements a commercial ozone generator with a known output per unit time was used in the recirculating system. For the humid air measurements solutions of sulphuric acid of varying concentration were placed in the closed system and twenty-four hours allowed for equilibrium conditions to be obtained. Air saturated with water vapor was obtained by running the output of a commercial aerosol humidifier directly into the test gap. Under these conditions water droplets condensed on all surfaces within the gap.

3.3. Measurement Technique

The meaningful interpretation of the breakdown data involves three experi-

mental considerations which are applicable to all of the reported results. These include: the establishment of an operational criterion for the breakdown lag time based on the observed pulse shapes, the removal of the statistical variation from the lag time data and a consideration of departures from similarity for data obtained with differing combinations of the breakdown parameters.

Figure (25) shows a typical pulse waveform provided by the current viewing resistor placed in the transmission line near the test gap. As the traveling wave passes the resistor the rise time of the wavefront AB is seen. As the wave continues passing the resistor and arrives at the gap the level portion BC is observed. When the wavefront reflected from the anode reaches the CVR (C to D on the trace) the waves traveling in two opposite directions cancel each other for a time given by DE. If breakdown does not occur in the gap the reflected wave continues and the trace is as shown in DEF. If there are initial electrons present in the gas space so that breakdown takes place, the gap will begin to conduct after a short delay DE. When breakdown is fully formed, reflection from the gap ceases and the pulse height returns to its previous level as indicated by the portion GH.

For the purposes of this study the point E, indicating the onset of breakdown is defined to correspond to a vertical deflection of one trace width above the base line of the trace. Further, we have measured formative time as the time between the instant the voltage reaches maximum on the anode (indicated by the point D in the observed pulse) and the time when the gap breaks down, E. Although these definitions are arbitrary, they are in accord with those used by other investigators.

The lag time DE is, in general, the sum of the formative and statistical lag times. The statistical delay time is caused by the finite rate of emission of electrons from the cathode surface and the statistical nature of the emission. Following the results of Strigel [10] and the analysis suggested by von Laue [11] the statistical time may be shown to obey an exponential distribution law. If the results of a number of measurements of the delay time for fixed voltage, pressure and gap distance are plotted on semilog axes with appropriate vari-

ables the exponential nature of the distribution may be seen. The statistical delay is described by

$$n_t = n_o e^{-t/\sigma}$$

where n_t is the number of time lags greater than t, n_o is the total number of events and σ is the mean statistical lag. Hence a semilog plot of n_t/n_o versus t should be a straight line yielding a value for σ from the slope and a value for the minimum delay, or the formative time, from the intercept at $n_t/n_o = 1$. Figure [26] shows four typical plots of actual measurements. Such plots have been made for all data reported here where use is made, on the average, of 27 data points for the measured lag time.

By the methods referenced above it is possible to use the information regarding σ to estimate the rate of electron emission from the ultraviolet irradiation of the cathode surface. Based on typical observed values of σ from the data the photoemission current for this experiment is approximately 5×10^{-10} amperes.

According to the theory the formative time may be described in terms of the variables $P\mathcal{Z}$ and E/P as in Equation (7). Similarity conditions should then apply in the sense that a particular value of E/P can be obtained from an unlimited number of combinations of the parameters: pressure, gap spacing and pulse voltage. In our experiments we have made an attempt to check similarity relationships. Hence our breakdown curves show data for different gap distances at all places where it was possible to obtain such data within limits imposed by theory and the experimental equipment. The breakdown curves are then drawn through the average of values determined from measurements on gaps of 0.051 to 6.0 cm. On the logarithmic plots used for viewing our data no significant departures from similarity laws were noted for the range of parameters used in our experiments.

4. Atmospheric Breakdown

4.1 Relation of DC to Microwave Fields

In the above two sections we have given details of the theoretical basis for describing nanosecond pulse breakdown and experimental results for a variety of gases. In this section we will make use of the theory and the results obtained in air to derive breakdown field strengths for short high power microwave pulses traversing the atmosphere. In particular we will calculate the field necessary for breakdown of the atmosphere from ground level to 100,000 feet as a function of frequency and pulse length.

In order to relate our results to microwave breakdown it is necessary to employ the concept of effective field for energy transfer defined as

$$E_e = \frac{E_o}{\left(1 + \frac{\omega^2}{\nu^2}\right)^{1/2}} \qquad (8)$$

Here E_e is the effective field, E_o is the rms microwave field, $\omega = 2\pi f$ where f is the microwave frequency and ν is the electron collision frequency. To a first approximation E_e is the effective field which would produce the same energy transfer as a steady field. Therefore, the data we obtain by dc video breakdown techniques may be converted to equivalent microwave data by means of this equation. It has, however, been found that the effective field as defined above is not able to account fully for all differences in energy transfer processes between various applied frequencies and dc video breakdown. Therefore, one additional normalization due to electron energy modulation will be used to render equivalent breakdown fields at various frequencies. This normalization is dependent on the product of gas pressure and wavelength ($p\lambda$) and is significant at $p\lambda$ values of 200 and greater[14].

In using the equation for effective field in the past it has been necessary to assume an average value of collision frequency dependent only on pressure i.e., for air $\nu_c = 5.3 \times 10^9 p$, where p is the pressure in mm Hg. It is well known, however, that the collision frequency is not independent of electron

energy [12] although, for the usual range of parameters covered, the approximation of energy independent collision frequency is sufficient. In the work reported here the electron energy changes as much as one hundred to one. Therefore, some correction for changed collision frequency is desirable. Fortunately, by comparing the results of two different nanosecond experiments, [12,13] it has been possible to approximate the energy dependence of the electron collision frequency.[12] The expression for electron collision frequency then becomes:

$$\nu_c = 5.3 \times 10^9 \, p + 1.15 \times 10^7 \, E_e \qquad (9)$$

Using the above factors we have converted our data taken with video pulses at E_e and at $p\lambda = 0$ to breakdown fields at some E_o and $p\lambda \neq 0$ corresponding to the appropriate frequency, pulse length and pressure.

The corrections necessary because of energy modulation are most significant at low frequency and high pressure when they amount to as much as a 15% lowering of the breakdown field. The change of collision frequency with field is significant only at the low pressure end of the breakdown curve at altitudes greater than 60 km where it amounts to as much as a factor of 10 lowering of the breakdown field.

4.2. The Atmospheric Model

In order to relate pressure and altitude so that we might determine breakdown field as a function of altitude we have made use of the U. S. Standard Atmosphere, 1962 [14]. We have converted the tabulated number density versus altitude to equivalent pressures at a temperature of 291 ^{o}K. A plot of pressure versus altitude so determined is shown in Figure (27). Perfect gas laws have been used in all calculations because they are more than 1% accurate over the range of pressure and temperature used here. Figure (27) represents the mean atmospheric density in the middle latitude regions (approximately 45^{o}). Systematic variability about this mean in the latitude region of 15^{o} to 60^{o} is also shown in Figure (27).

Atmospheric molecular weight is constant to 1 part in 10^5 over the altitude range of interest here [14]. Hence, we are safe in extending the data taken in air at sea level to the atmosphere. Ozone which has its maximum concentration in the 20 to 40 km altitude range amounts to only 1 part in 10^4 to 10^6 of the atmosphere in this range [15]. Its effect on atmospheric breakdown will therefore be negligible (see section 3.4 above).

The effects of atmospheric water vapor on breakdown fields have not been treated here. Recent data [12] and above Section 3.4 has indicated that the vapor alone is not significant in changing breakdown fields. The problem of propagation through condensed vapor (clouds) is not treated here.

The result of combining the standard atmosphere data with the breakdown field data is shown in Figures (28, 29, 30 and 31). These figures show the breakdown field for 1, 3, 9 and 27 gc as a function of altitude for various pulse lengths between 1 and 100 nanoseconds.

We define breakdown here to mean that the gas (atmosphere) begins to conduct appreciable current during the pulse duration. As noted above, this is the definition used to define formative time for breakdown in our dc measurements.

4.3. Radar System Design Considerations

These figures (28 thru 31) are intended for use by the radar system designer to indicate upper limits on allowable field strengths. In calculating the breakdown fields and plotting them in this manner we tacitly assume that there are free electrons available to initiate the breakdown process. Under certain circumstances such as in the vicinity of a re-entry body, or at high latitudes during periods of solar activity this assumption is a very good one. On the other hand at low altitudes (20-50 km) and low latitude the free electron concentration is very low [16]. Here the principal source of free electrons is cosmic radiation. Hence the net free electron concentration is low.

Assuming the electron concentration is sufficient to initiate breakdown, the curves of Figures (28-31) represent an upper limit on the breakdown field strength. In the real case for short pulse extremely narrow beam airborne

radars it may be that breakdown is unlikely because of a statistical lack of electrons within the radar beam. In such cases it will be necessary to carry out detailed calculations involving the radar parameters and electron production and decay rates in the atmosphere.

In order to indicate the inherent variability of the breakdown curves the results at 3 gc for pulses of 1.0 and 100 ns have been shown with the variations to be expected due to altitude density fluctuations. The upper and lower limits of these curves represent the range of systematic variability due to seasonal changes in the 15° to 60° latitude range. Curves for other pulse lengths and frequencies will have the same variability at equal altitudes. The important point to note is that the minimum of each curve will change altitude value no more than $\pm$ 3% and hence the curves based on the standard atmosphere alone are sufficient for ordinary purposes.

The breakdown data from which these curves are obtained was deliberately taken at a variety of pressures, field strengths and characteristic dimensions. Hence the average curve obtained from this data takes into account actual variations which may exist in the similarity parameters. It is interesting to note that gap width used varied between 6.0 and 0.13 cm while quarter wavelengths for the frequencies calculated varied between 7.5 and 0.28 cm. Similarly gap pressures varied between 760 and 1 mm Hg while calculated pressures vary between 760 and .06 mm Hg. Hence experimental conditions are close enough to the calculated results to allow a high degree of confidence in the validity of the resultant breakdown curves. Finally it should be noted that although previous work [17] has predicted breakdown for pulses of 50 and 100 ns length these predictions were based on extrapolations of data obtained with 0.8 microsecond pulses and longer. Our work, on the other hand, has used pulses of 0.5 to 20 nanoseconds exclusively and hence is based directly on empirical data rather than extrapolation.

Table II is a tabulation of the breakdown field strengths at the earth's surface as a function of pulse length and frequency. In using this table the radar designer should remember that these are the free field voltage breakdown

levels. In the vicinity of wave guides, feed horns, antennae etc. the field strength and breakdown problem will have to be treated as a boundary value problem.

5. Summary

A consistent picture of dc nanosecond breakdown has been given. Based on microwave theory we have developed the analytical framework for describing dc nanosecond breakdown, within certain prescribed limits purely in terms of gas parameters. Further we have comprared quantitatively this description with experimental results and found them in agreement. Additionally we have related earlier microwave breakdown studies to our work and have shown that our work is not only an extension of earlier microwave work but may be quantitatively related to microwave breakdown through the concept of effective field.

We have applied our results to three practical problems. First, we have obtained breakdown data in a number of common insulating gases. This is particularly important since breakdown curves for these gases cannot be calculated because of the lack of basic data. Secondly, we have derived, on the basis of our breakdown measurements, basic data about two of these insulating gases. Finally we have applied the breakdown results in air obtained by our method and pulsed microwave methods to the problem of determining breakdown field strength as a function of altitude, frequency and pulse width.

APPENDIX I

Calculation of Theoretical Breakdown Curves

Theoretical breakdown curves have been calculated for five of the nine test gases. These curves are based on the breakdown equation [7] and available data in the manner outlined below.

Examination of the equation shows that a knowledge of two gas discharge parameters are necessary for the calculation of the $P\tau$ versus E/P curves. Specifically electron drift velocity and net ionization coefficients ($(\alpha - \beta)/P$) are needed as a function of E/P in order to calculate $P\tau$. Table III gives a summary of the range of the range of drift velocity and $(\alpha - \beta)/P$ data available from the literature as a function of E/P.

It is apparent from the table that the range of drift velocity data is much more limited then the range of $(\alpha - \beta)/P$ data. We have therefore found it necessary to extrapolate the measured drift velocity data so that its range would be the same as the net ionization coefficient data. For this purpose we have plotted available drift velocity data for the five gases versus E/P and have made a graphical linear extrapolation of the data. (Fortunately for three of the gases we have very modern data [29,23] available from experiments done on a time scale similar to our own.) The analytic expression satisfying the linear extrapolation of existing drift velocity data is shown in Table III for each of the five gases. This expression along with measured values of $(\alpha - \beta)/P$ is used in calculating each breakdown curve.

The range of available α/P or $(\alpha - \beta)/P$ data along with the reference is shown in Table III for each gas. Not all available references were used because in many cases the differing references are not self consistent. It may be noted that some gases use both modern and older references. Where no choice was possible older references were used for the high E/P range. This is because of the lack of good vacuum equipment and subsequent contamination (mercury vapor) of results for measurements of α/P or $(\alpha - \beta)/P$ for low E/P.

In all cases our own data covers a wider range of E/P than may be calculated from available data. Hence the breakdown data may be used to obtain the net ionization coefficient or drift velocity for high E/P if either of the other quantities is known.

APPENDIX II

Calculation of $(\alpha - \beta)/P$ for Freon 12 and Sulpher Hexafluoride

As described above (Appendix I) Equation (7) plus drift velocity and $(\alpha - \beta)/P$ data may be used to calculate the theoretical breakdown curve. However, for Freon 12 and SF_6 drift velocity data is not available while only limited $(\alpha - \beta)/P$ data is available. We have, therefore, used our breakdown data and iterative techniques to establish first electron drift velocity in the range where $(\alpha - \beta)/P$ data are available and second with the value of drift velocity vs E/P so determined find the $(\alpha - \beta)/P$ values which satisfy our breakdown results at high E/P values.

Table III lists the derived electron drift velocities. For SF_6 it was necessary to extrapolate the measured values of $(\alpha - \beta)/P$ to an E/P of 200 because of uncertainties in our breakdown curves at the lower E/P values. Figures (32) and (33) show both the derived $(\alpha - \beta)/P$ curves and the $(\alpha - \beta)/P$ curves taken from the references. As a test of the accuracy of data on $(\alpha - \beta)/P$ so obtained, a calculation using the identical technique was performed on air. The resulting $(\alpha - \beta)/P$ curve had the same shape and peaked at the same E/P value as the directly measured data and was within a factor of two of the absolute value.

REFERENCES

1. A. D. MacDonald and S. C. Brown, Phys. Rev. 75, 411 (1949)
2. M. A. Herlin and S. C. Brown, Phys. Rev. 74, 291 (1948)
3. S. C. Brown and A. D. MacDonald, Phys. Rev. 76, 1629 (1949)
4. L. Gould and L. W. Roberts, J. Appl. Phys. 27, 1162 (1956)
5. R. C. Fletcher, Phys. Rev. 76, 1501 (1949)
6. H. Raether, Elktrotech Zeitr. 63, 301 (1942)
7. F. R. Dickey, J. Appl. Phys. 23, 1336 (1952)
8. R. C. Fletcher, Rev. Sci. Instr. 20, 861 (1949)
9. W. Rogowski, Arch. f. Elekt. 16, 73 (1926)
10. K. Stringel, Arch. f. Elekt. 26, 831 (1932)
11. M. von Laue, Ann. Phys. Lpz. 76, 261 (1925)
12. C. Buntschuh and M. Gilden, RADC-TDR-64-204 (July 1964)
13. P. Felsenthal and J. M. Proud, RADC-TDR-64-38 (March 1964)
14. NASA, U. S. Air Force, U. S. Weather Bureau, U. S. Standard Atmosphere 1962, Washington, D. C. (December 1962)
15. R. D. Rawcliffe, G. E. Meloy, R. M. Friedman, and E. H. Rogers, J. Geophys. Res. 68, 6425 (1963)
16. M. Nicolet and A. C. Aiken, J. Geophys. Res. 65, 1469 (1960)
17. A. D. MacDonald, Proc. IRE 47, 436 (1959)
18. M. A. Harrison and R. Geballe, Phys. Rev. 91, 1 (1953)
19. M. J. Druyvesteyn and F. M. Penning, Rev. Mod. Phys. 12, 87 (1940)
20. K. Masch, Arch. f. Elekt. 26, 582 (1932)

21. J. S. Townsend, Motions of Electrons in Gases (Clarendon Press 1925)

22. R. A. Nielson and N. E. Bradbury, Phys. Rev. 51, 69 (1937)

23. A. von Engel, Handbuch der Physik (Springer Verlag, Berlin 1956) XXI p 504

24. K. H. Wagner, Zeit. f. Physik 178, 64 (1964)

25. A. von Engel and M. Steenbeck, Elektrische Gaseutladungen (Springer Verlag, Berlin 1932) p 106

26. R. A. Nielson, Phys. Rev. 50, 950 (1936)

27. J. A. Hornbeck, Phys. Rev. 83, 374 (1951)

28. M. S. Bahalla and J. D. Craggs, Proc. Phys. Soc. 80, 151 (1960)

29. L. Frommhold, Zeit. f. Physik 160, 554 (1960)

30. A. E. D. Heylen, Nature 183, 1545 (1959)

TABLE I

Ranges of Variables Used for Experiments Reported Here

Gas	Voltage Range (kv)	Pressure Range (mm Hg)	Gap Distance (cm)	Purity (Per Cent)	Measured Formative Time (ns)
Air	5 to 30	1.0 to 760	0.13 to 6.0	Laboratory	0.5 to 18
Nitrogen	4 to 20	1.0 to 780	0.13 to 6.0	99.78	0.4 to 25
Oxygen	5 to 25	1.0 to 760	0.18 to 6.0	99.5	0.8 to 19
Argon	4 to 25	1.0 to 760	0.18 to 6.0	99.997	0.8 to 15
Helium	5 to 25	2 to 464	0.50 to 6.0	99.996	0.4 to 18
SF_6	4 to 25	1.0 to 750	0.051 to 6.0	98.7	0.4 to 19
Freon 12	7 to 25	1.0 to 500	0.051 to 6.0	99.9	0.3 to 11.5
Freon 114	7 to 25	1.0 to 760	0.051 to 6.0	99.9	0.4 to 17.5
Freon C318	7 to 25	1.0 to 700	0.051 to 6.0	99.5	0.8 to 11

TABLE II

Microwave Breakdown Fields at the Earth's Surface

as a Function of Pulse Length and Frequency

Pulse Length	1 gc	3 gc	9 gc	27 gc
10^{-9} s	7.68×10^4	7.68×10^4	7.75×10^4	7.91×10^4
5×10^{-9} s	4.96×10^4	4.96×10^4	5.04×10^4	5.2×10^4
10^{-8} s	4.19×10^4	4.19×10^4	4.26×10^4	4.42×10^4
5×10^{-8} s	2.94×10^4	2.94×10^4	3.10×10^4	3.26×10^4
10^{-7} s	2.56×10^4	2.56×10^4	2.71×10^4	2.87×10^4 v/cm

TABLE III

Gas Discharge Parameters and References Used to Develop Theoretical Breakdown Curves

Gas	Range of Applicable Drift Velocity Data (E/P)	Reference	Adopted Linear Extrapolation to Drift Velocity Data (cm/sec.)	Range of $(\alpha-\beta)/P$ Data (E/P)	Reference
Air	0.5 - 20 0.5 - 100	22 21	$7 \times 10^6 + 2 \times 10^5$ E/P	50 - 67 67 - 300 300 - 1000	18 19
Nitrogen	40 - 200	24	2.9×10^5 E/P	40 - 100 100 - 500 500 - 2000	30 20 23
Oxygen	40 - 125	29	$14 \times 10^6 + 1.4 \times 10^5$ E/P	40 - 66.7 66.7 - 350	18
Argon	15 - 42	24	$10^6 + 2 \times 10^5$ E/P	30 - 1500	19
Helium	0.5 - 45	26, 27	7.6×10^5 E/P	10 - 100	19
SF_6			0.71×10^5 E/P (See Appendix II)	90 - 160	28
Freon 12			0.33×10^5 E/P (See Appendix II)	135 - 250	18

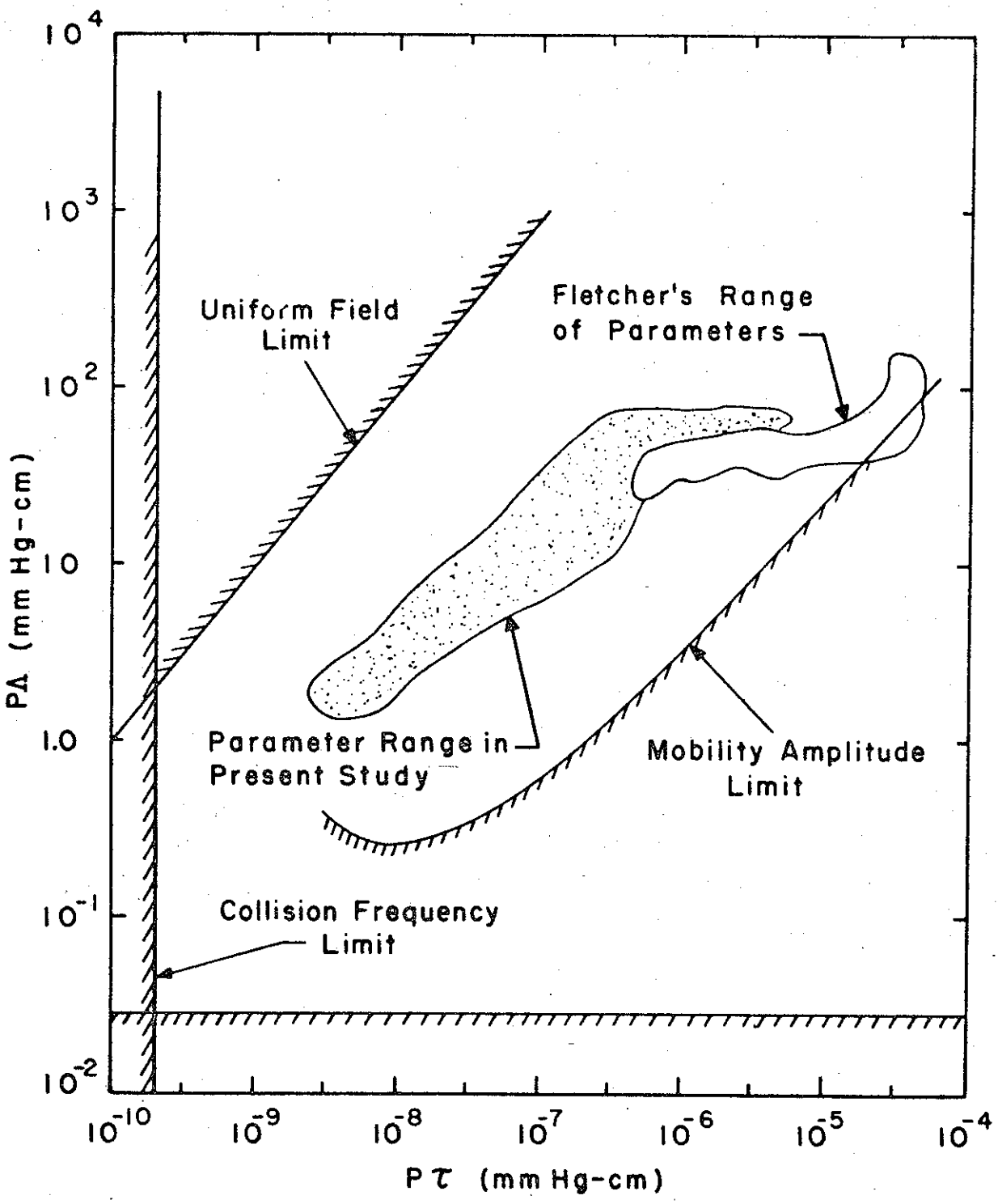

FIGURE 1.

VALIDITY LIMIT LINES FOR AIR

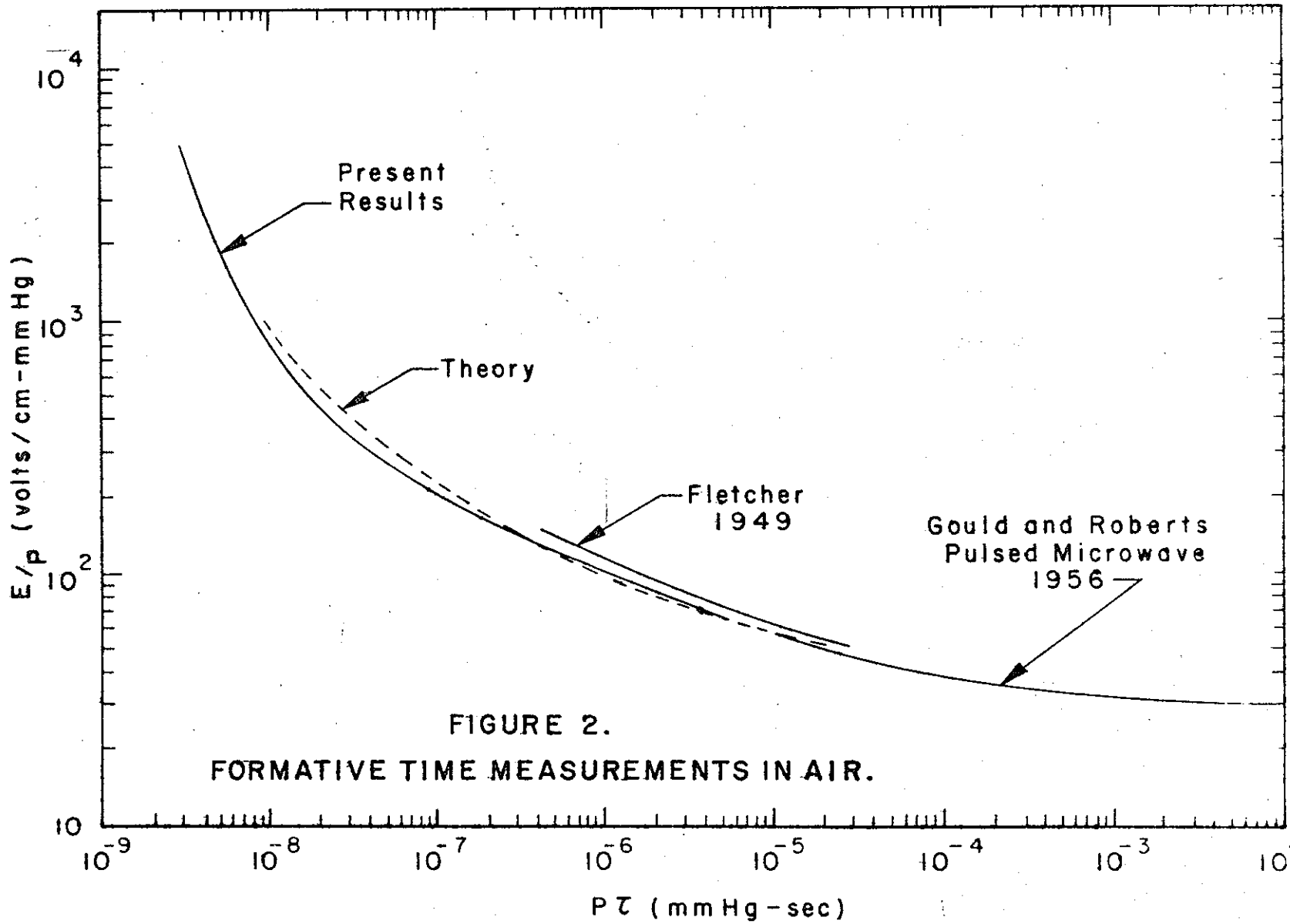

FIGURE 2.

FORMATIVE TIME MEASUREMENTS IN AIR.

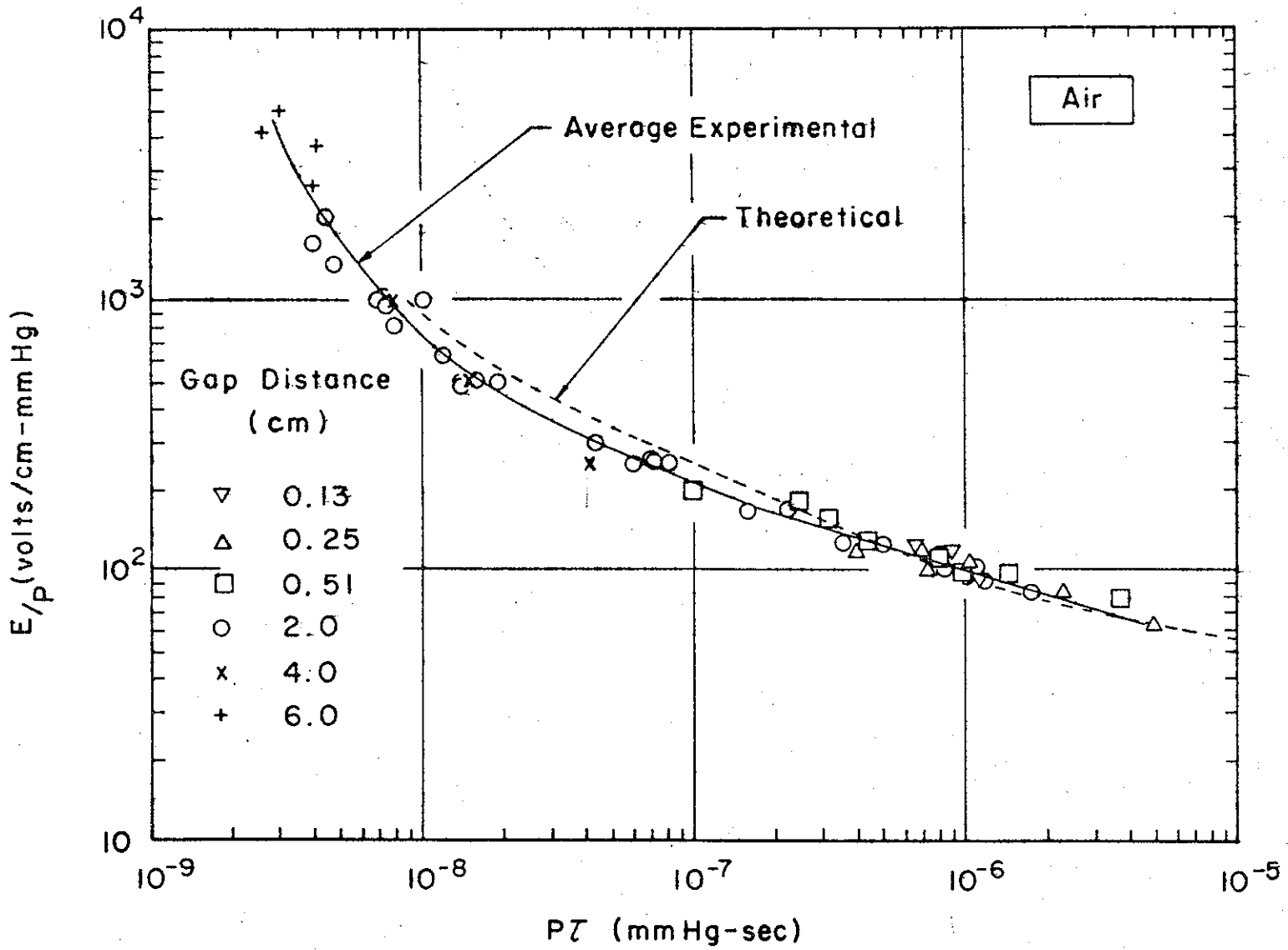

FIGURE 3.

AIR EXPERIMENTAL AND THEORETICAL BREAKDOWN CURVES AND DATA

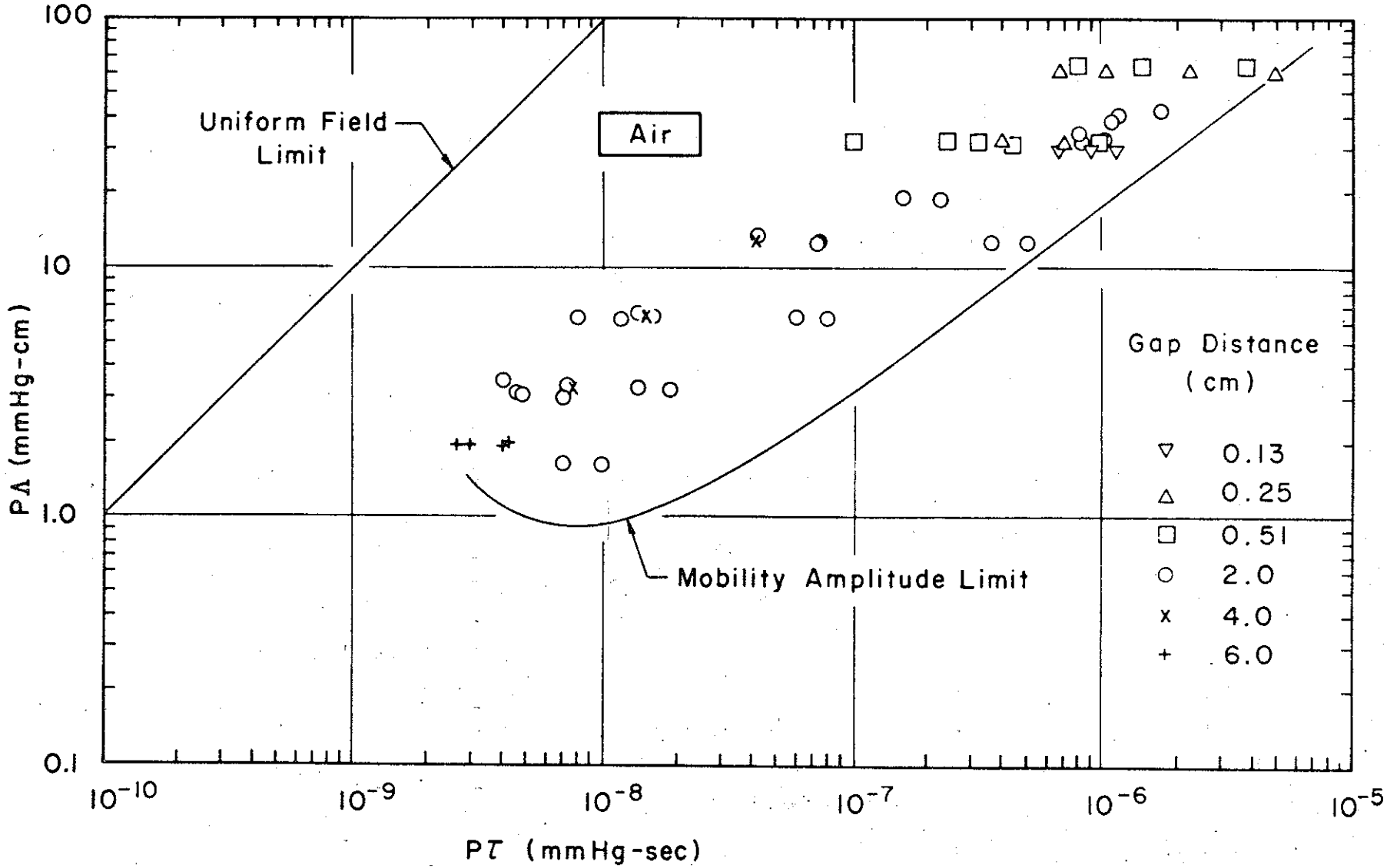

FIGURE 4.

AIR EXPERIMENTAL DATA IN RELATION TO THEORY LIMITS.

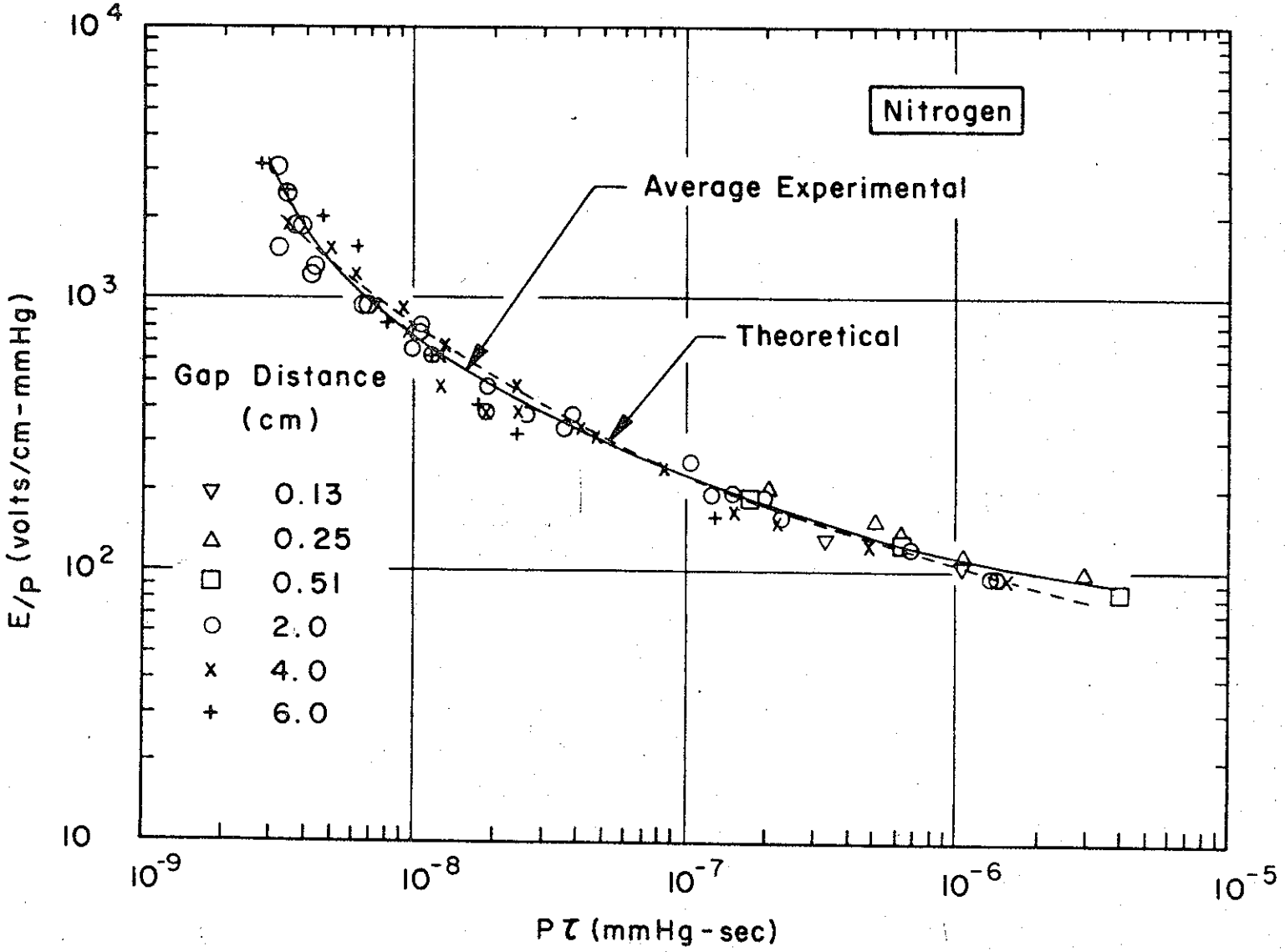

FIGURE 5.

NITROGEN EXPERIMENTAL AND THEORETICAL BREAKDOWN CURVES AND DATA.

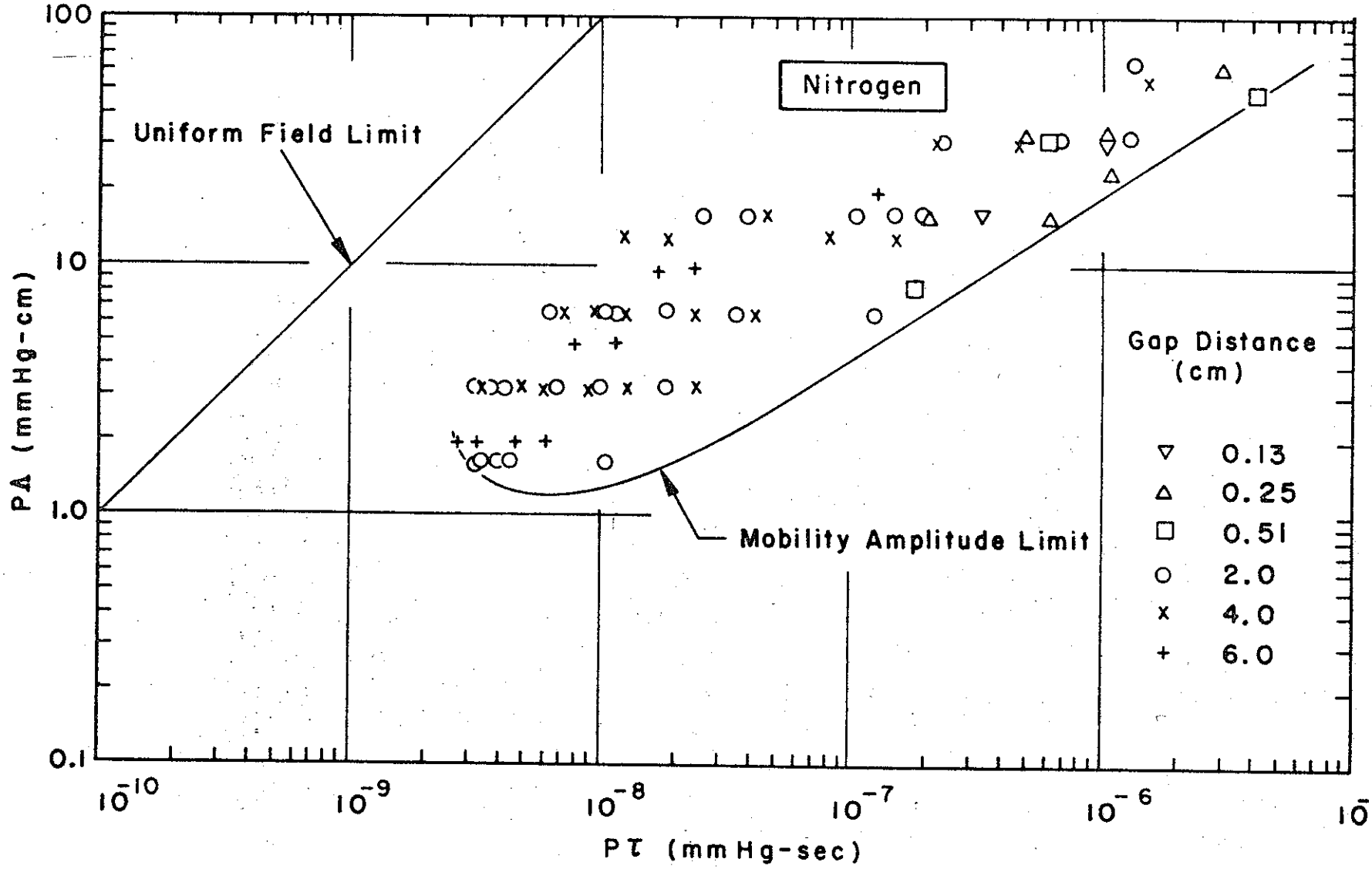

FIGURE 6.
NITROGEN EXPERIMENTAL DATA IN RELATION TO THEORY LIMITS.

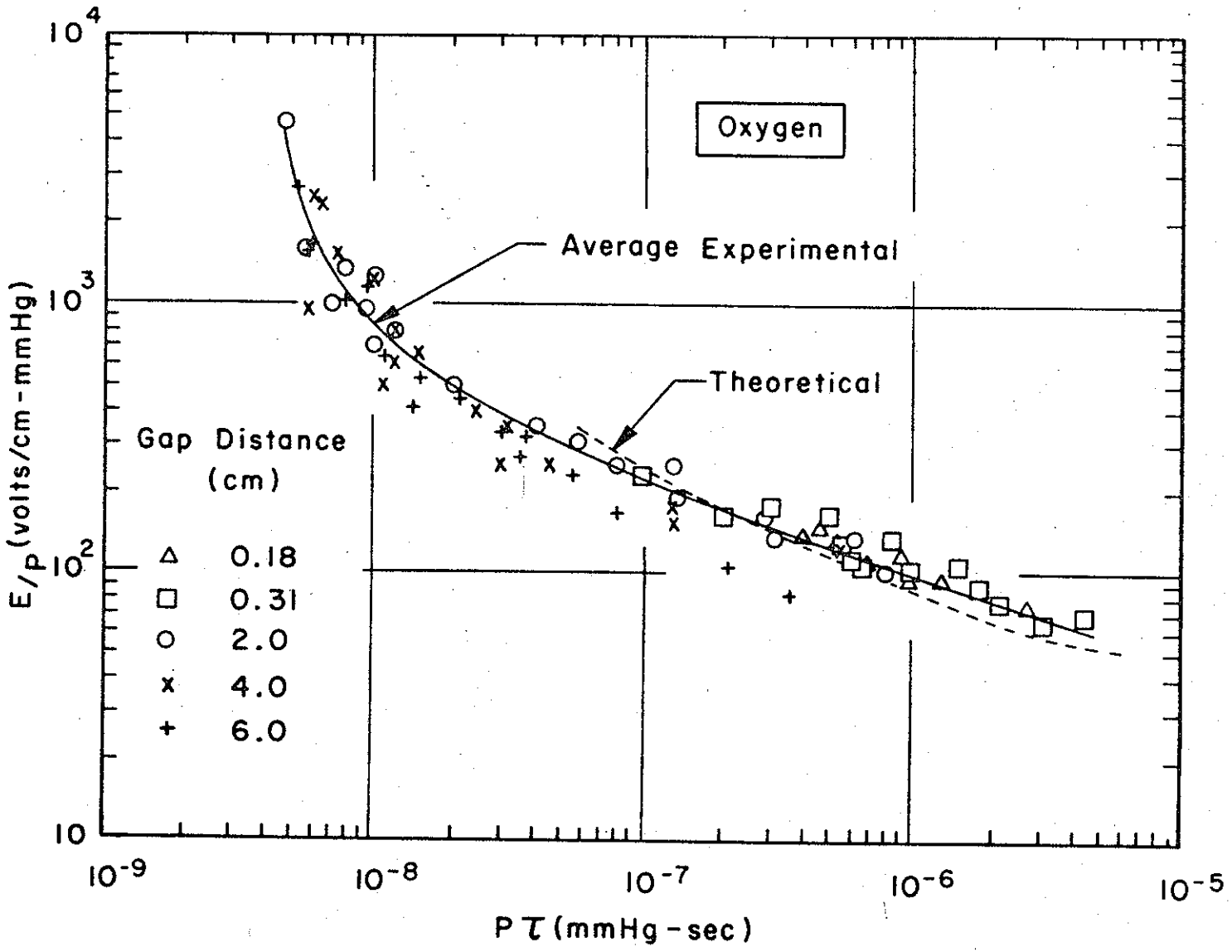

FIGURE 7.

OXYGEN EXPERIMENTAL AND THEORETICAL BREAKDOWN CURVES AND DATA.

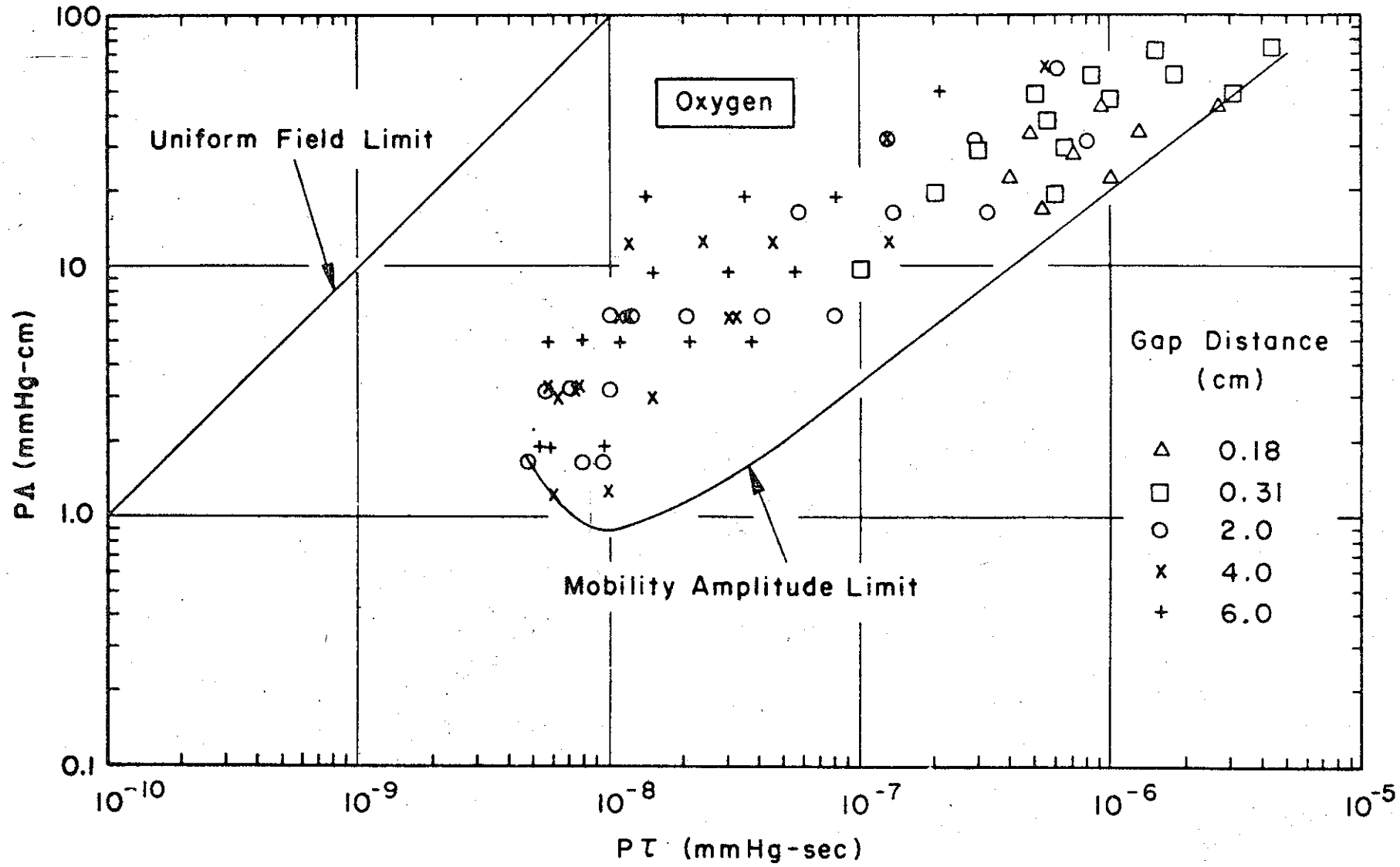

FIGURE 8.

OXYGEN EXPERIMENTAL DATA IN RELATION TO THEORY LIMITS.

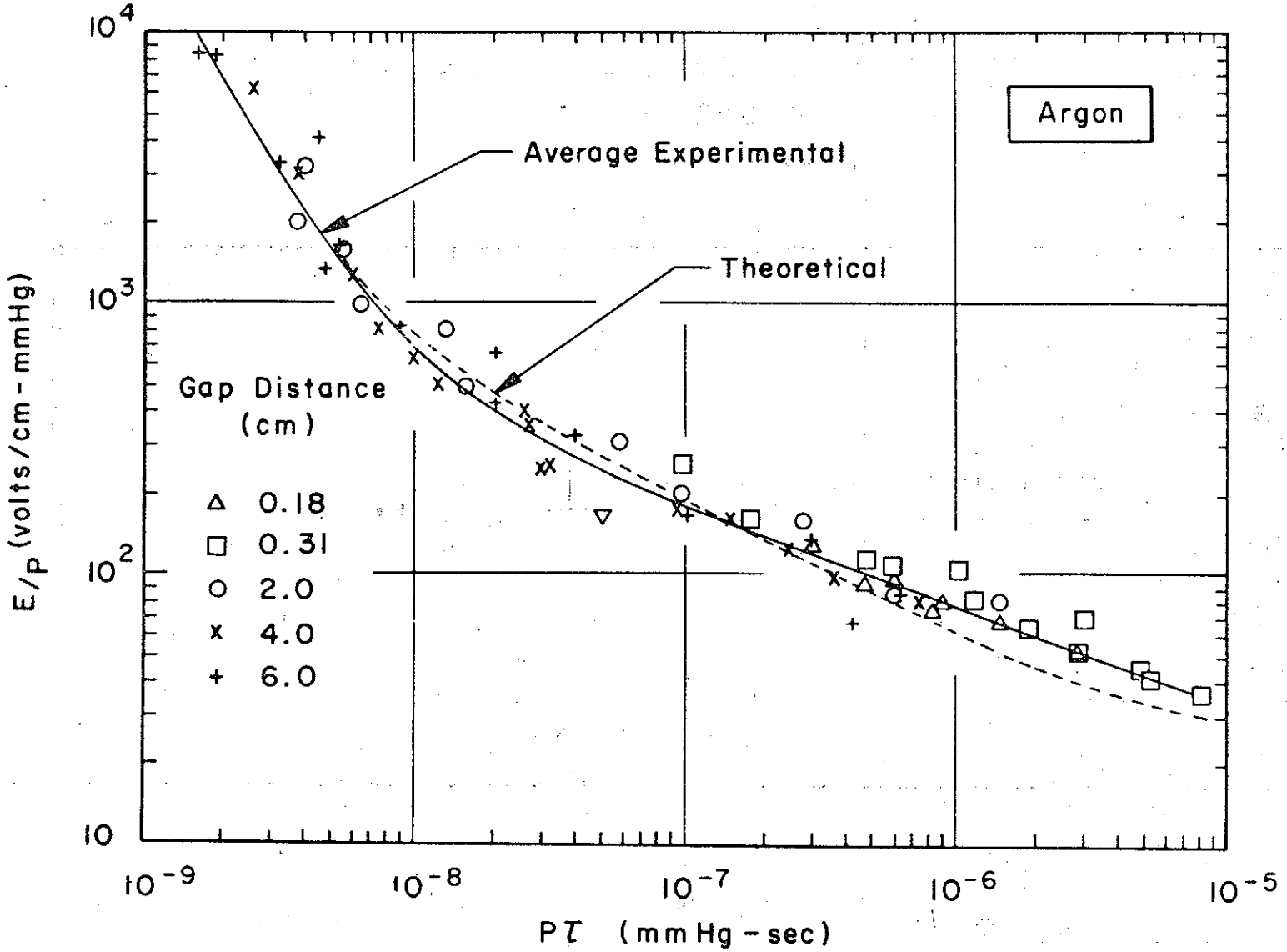

FIGURE 9.

ARGON EXPERIMENTAL AND THEORETICAL BREAKDOWN CURVES AND DATA.

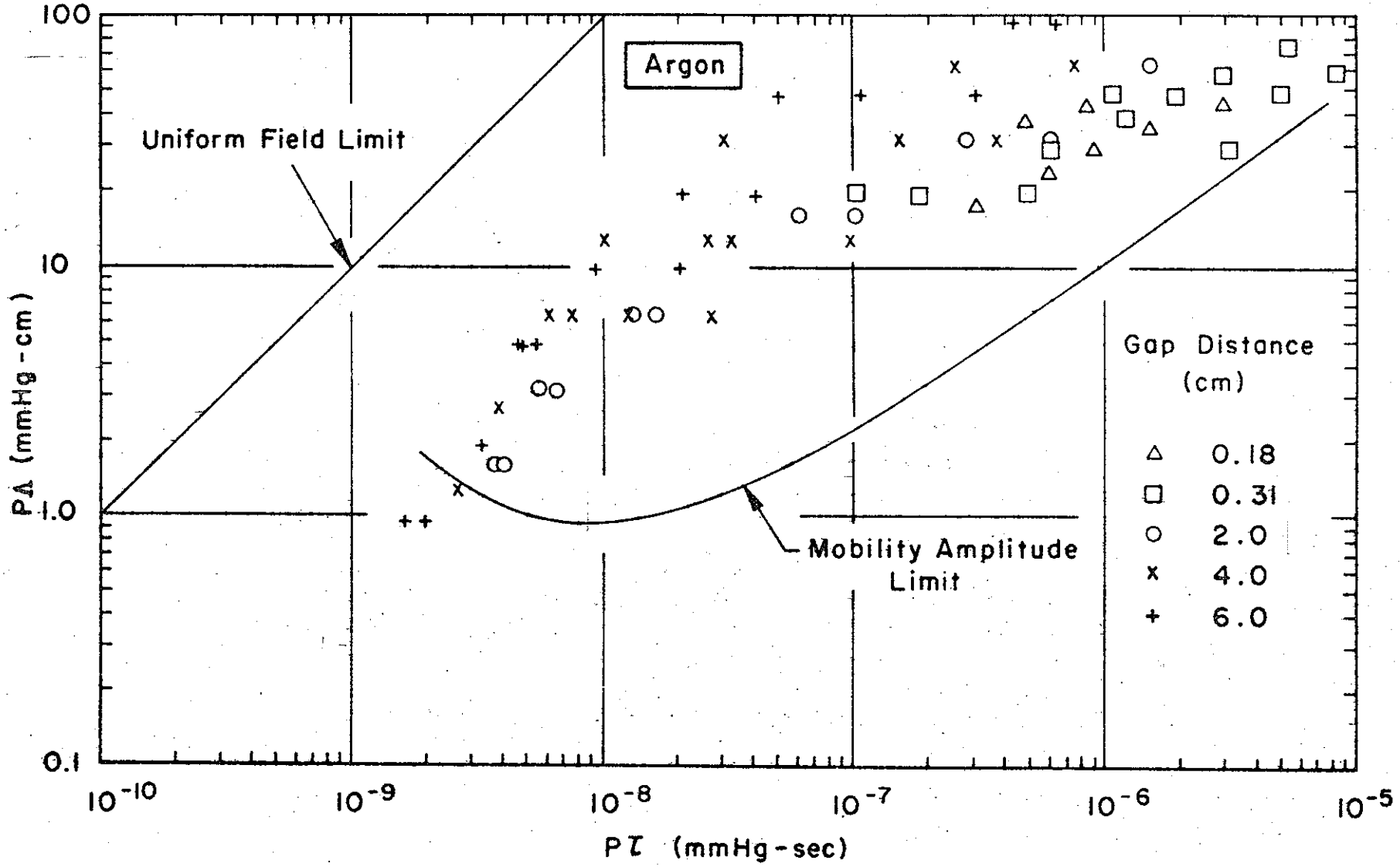

FIGURE 10.

ARGON EXPERIMENTAL DATA IN RELATION TO THEORY LIMITS.

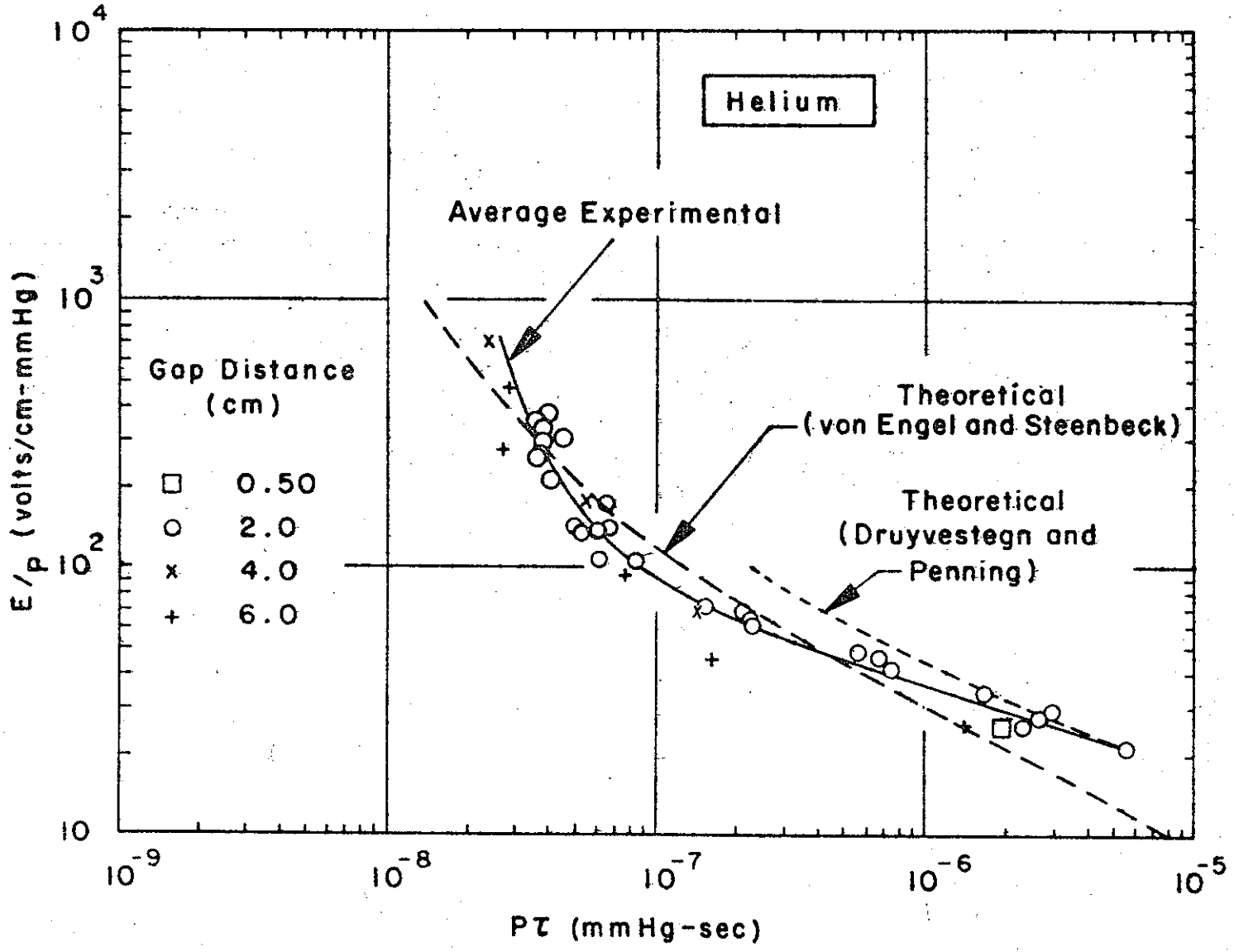

FIGURE II.

HELIUM EXPERIMENTAL AND THEORETICAL BREAKDOWN DATA AND CURVES.

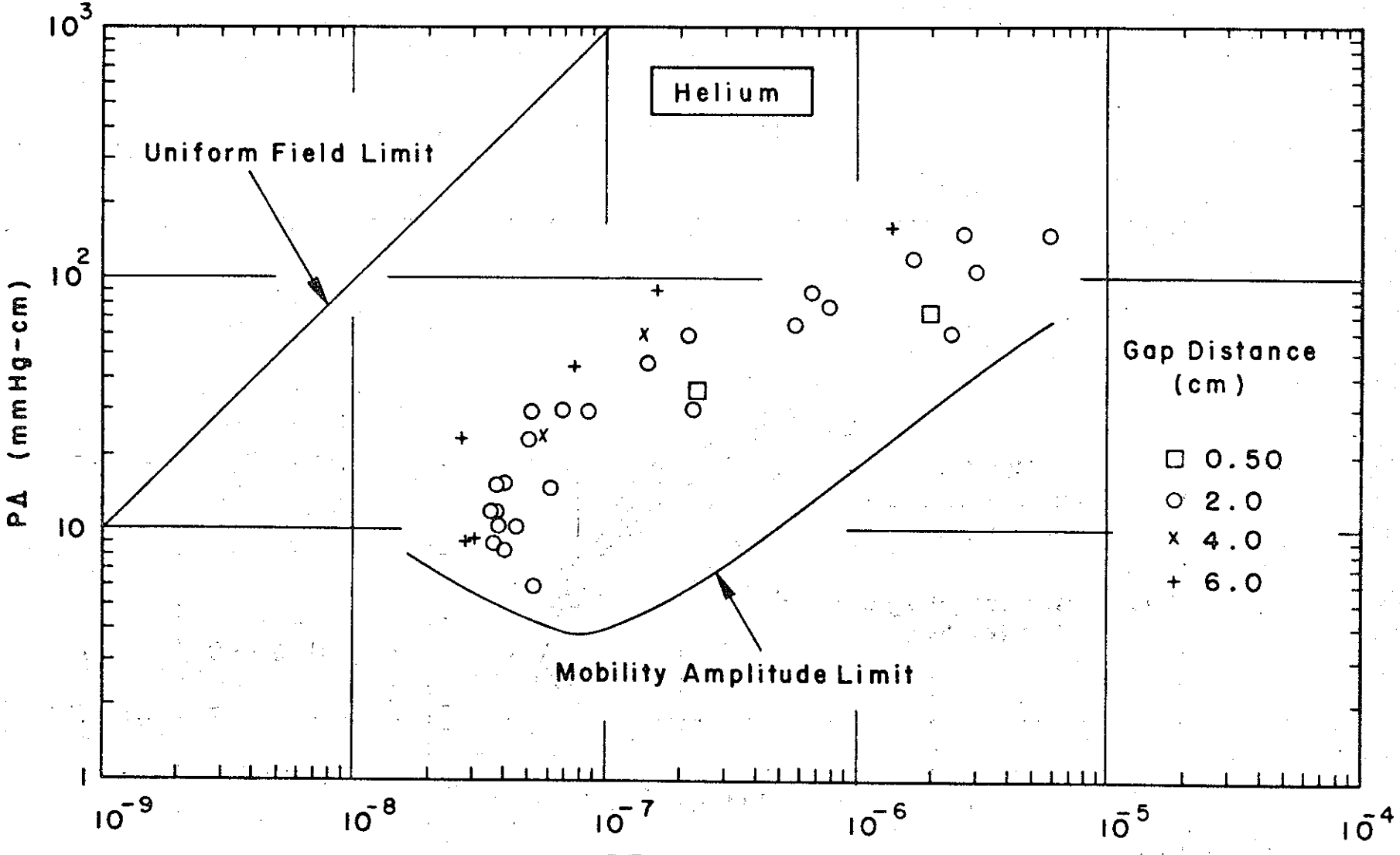

FIGURE 12.

HELIUM EXPERIMENTAL DATA IN RELATION TO THEORY LIMITS.

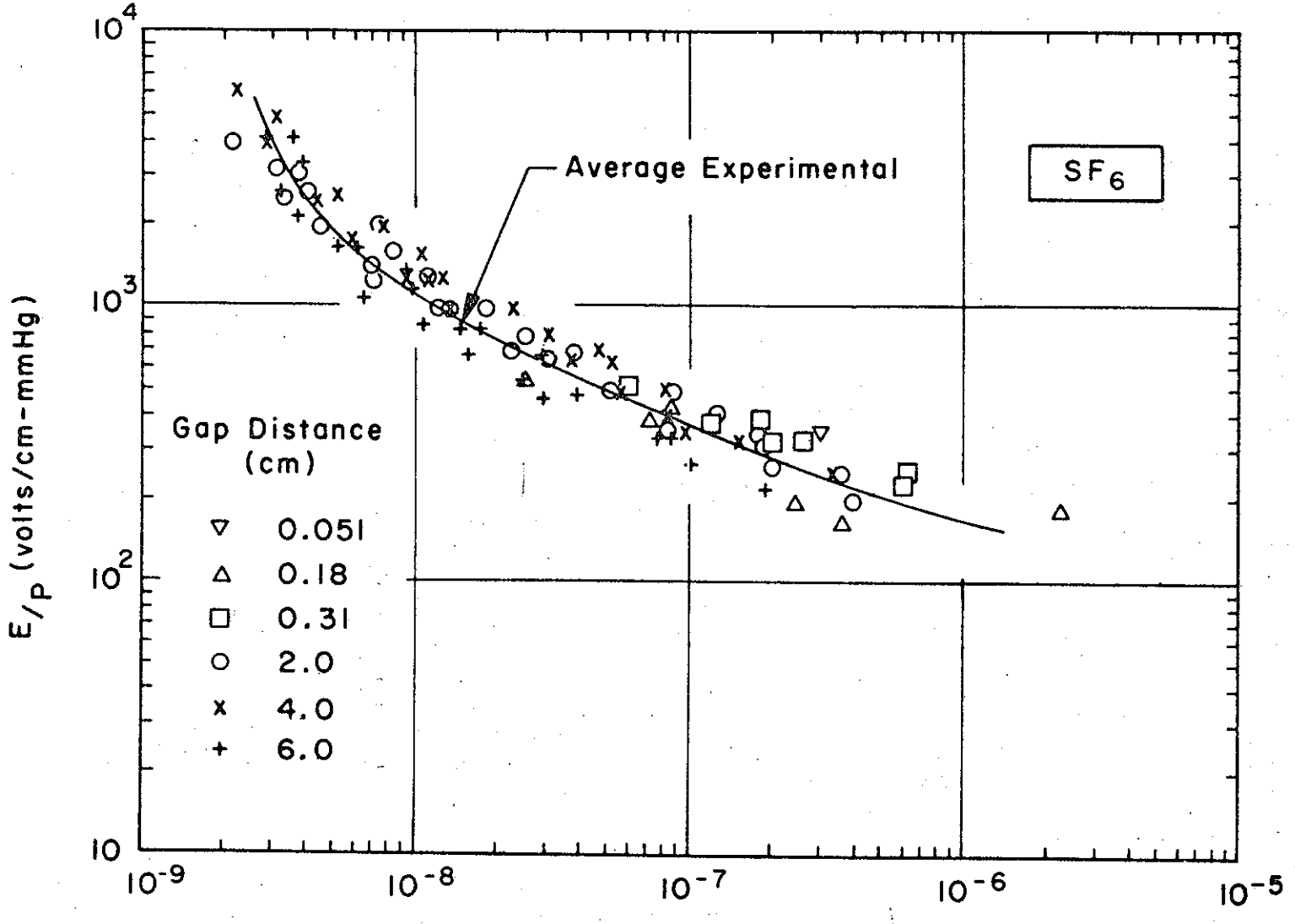

FIGURE 13.

SULPHUR HEXAFLUORIDE EXERIMENTAL BREAKDOWN CURVE AND DATA.

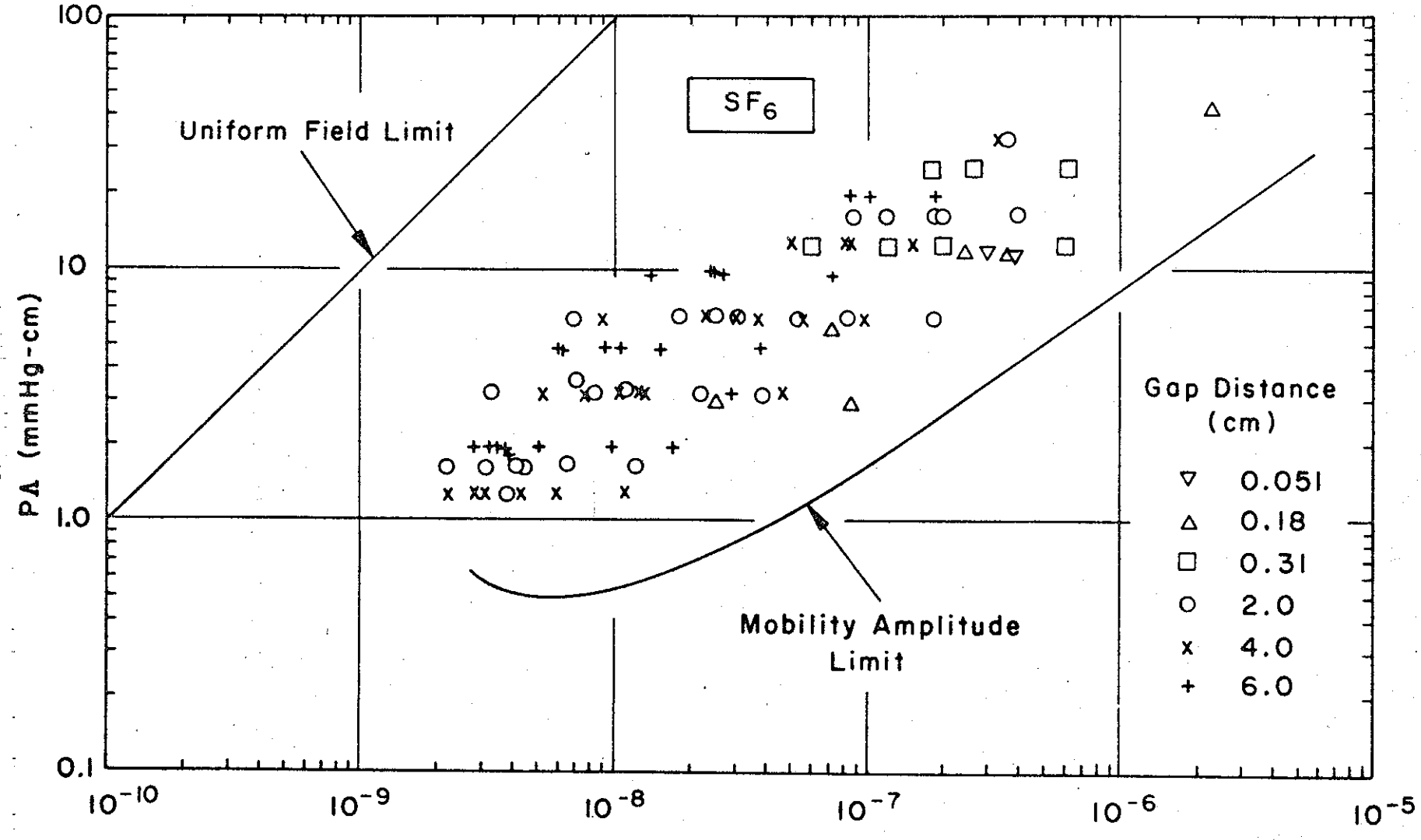

FIGURE 14.

SULPHUR HEXAFLUORIDE EXPERIMENTAL DATA IN RELATION TO THEORY LIMITS.

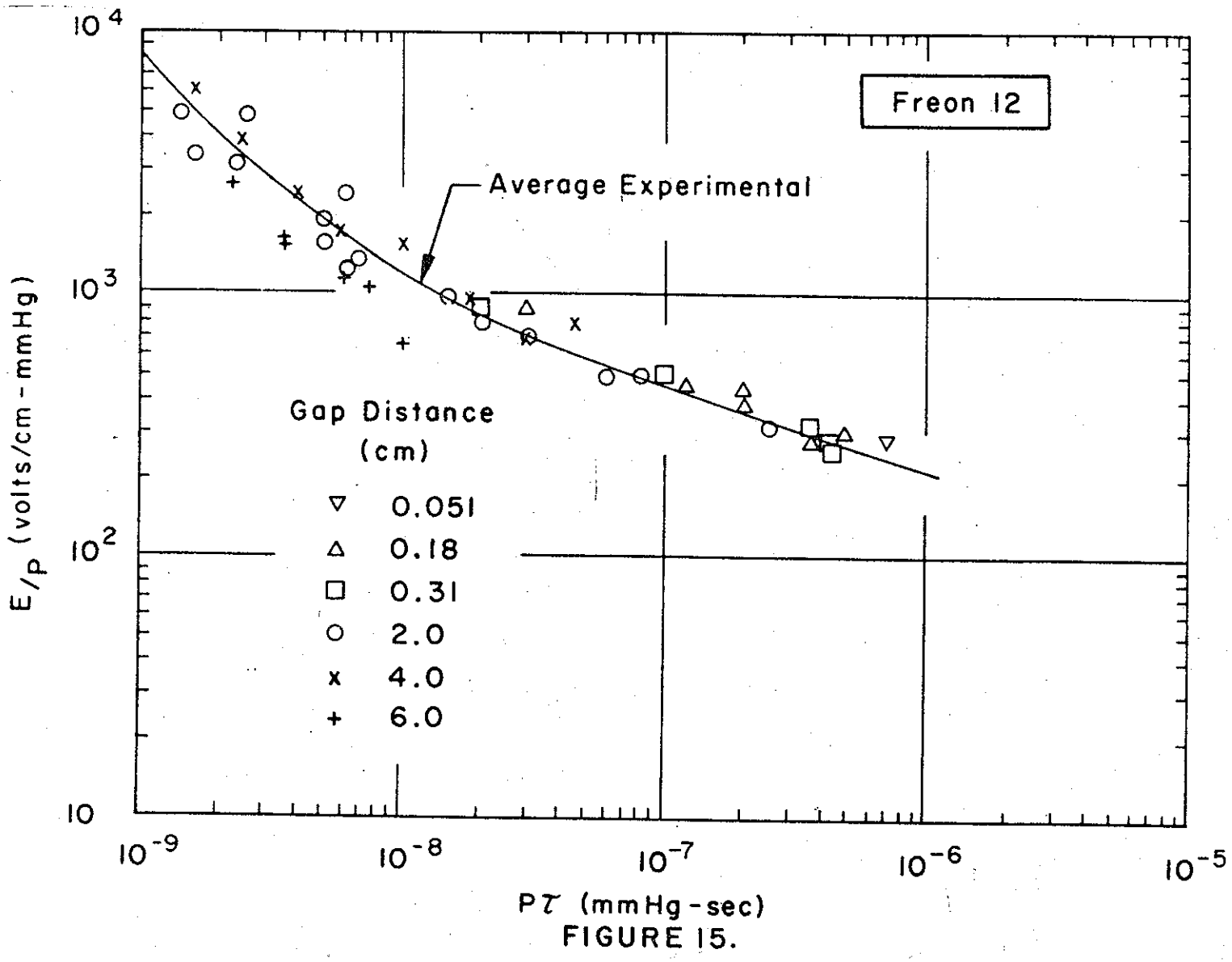

FIGURE 15.

FREON 12 EXPERIMENTAL BREAKDOWN CURVE AND DATA.

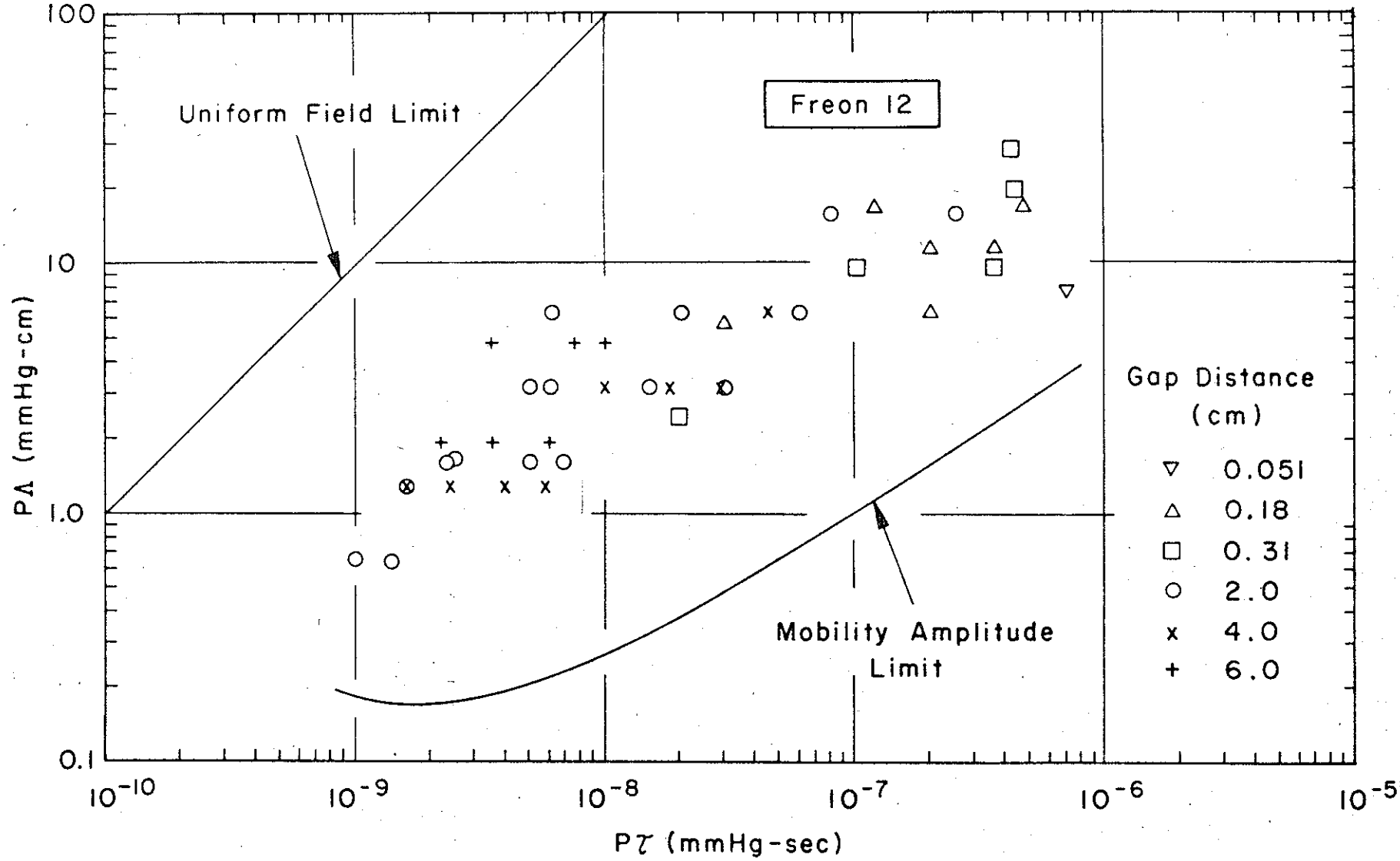

FIGURE 16.

FREON 12 EXPERIMENTAL DATA IN RELATION TO THEORY LIMITS.

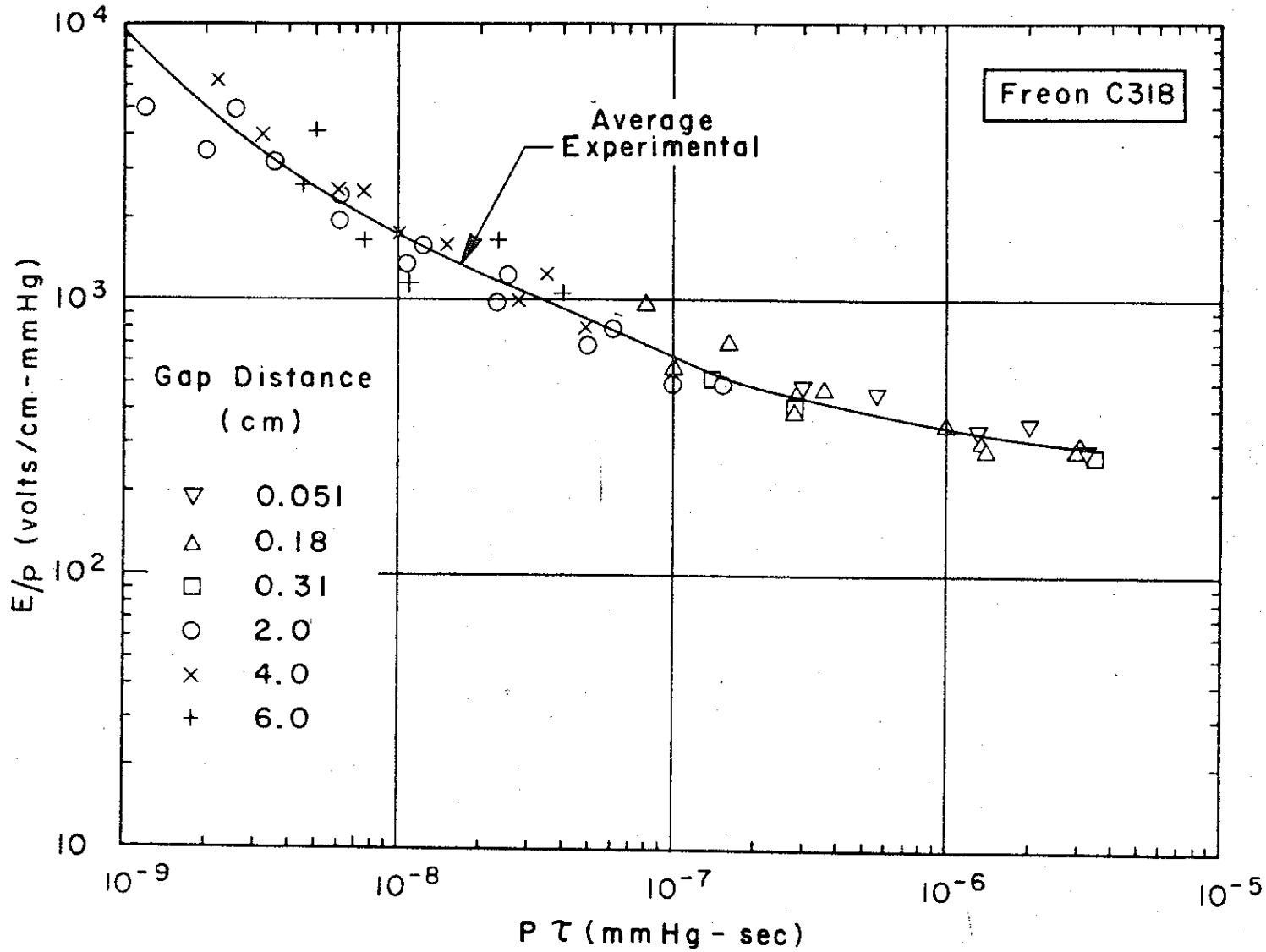

FIGURE 17.

FREON C318 EXPERIMENTAL BREAKDOWN CURVE AND DATA.

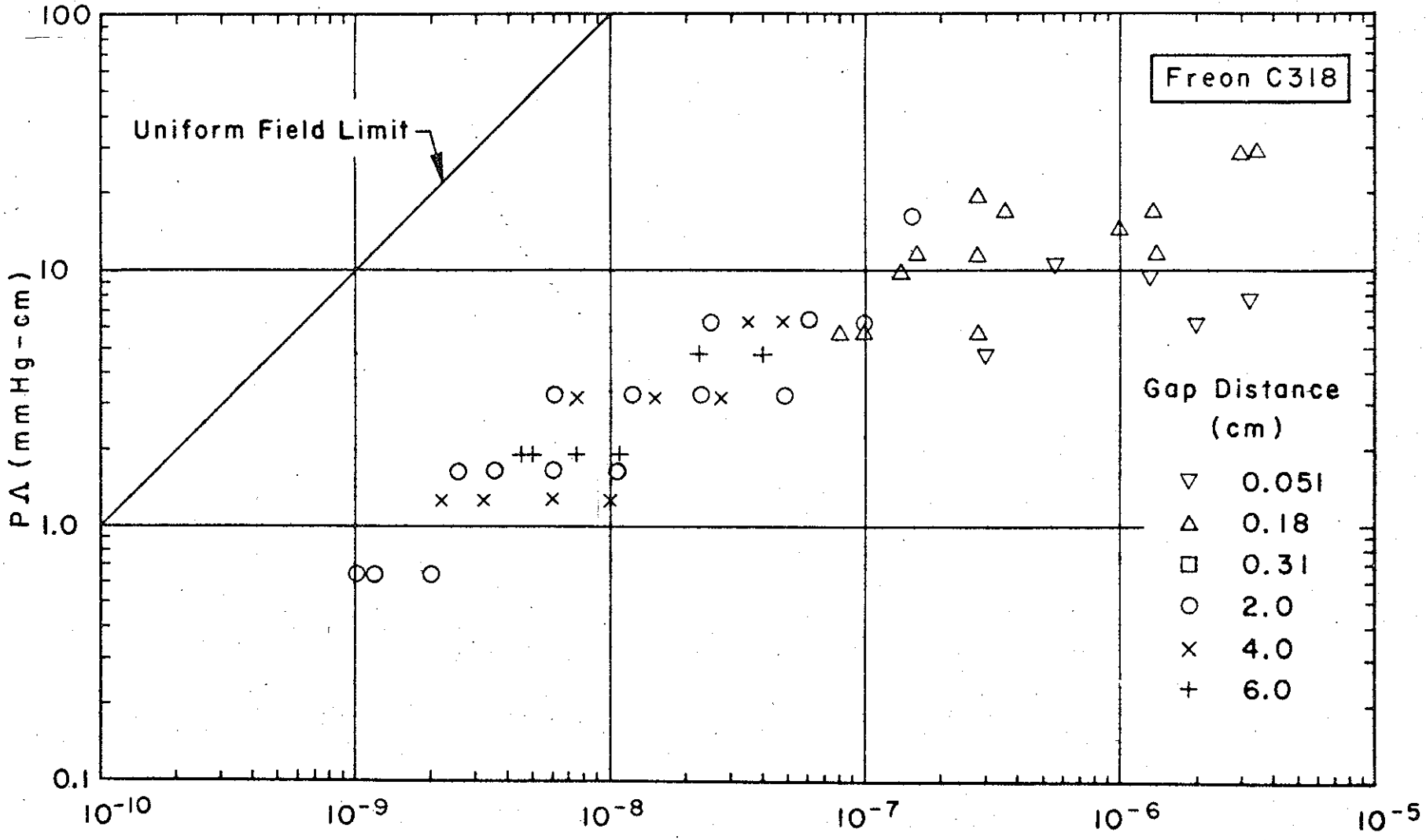

FIGURE 18.

FREON C318 EXPERIMENTAL DATA IN RELATION TO THEORY LIMITS.

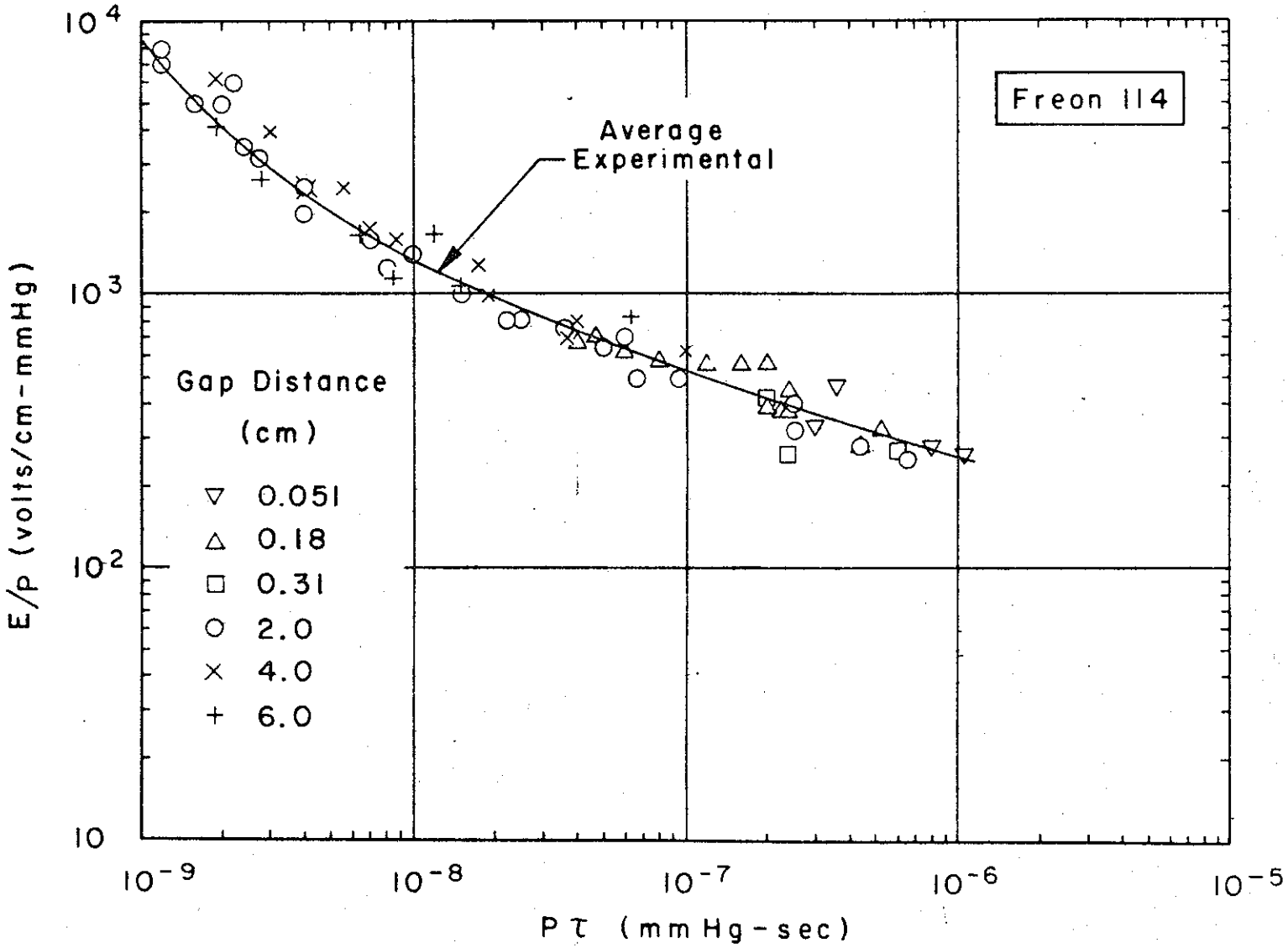

FIGURE 19.

FREON 114 EXPERIMENTAL BREAKDOWN CURVE AND DATA

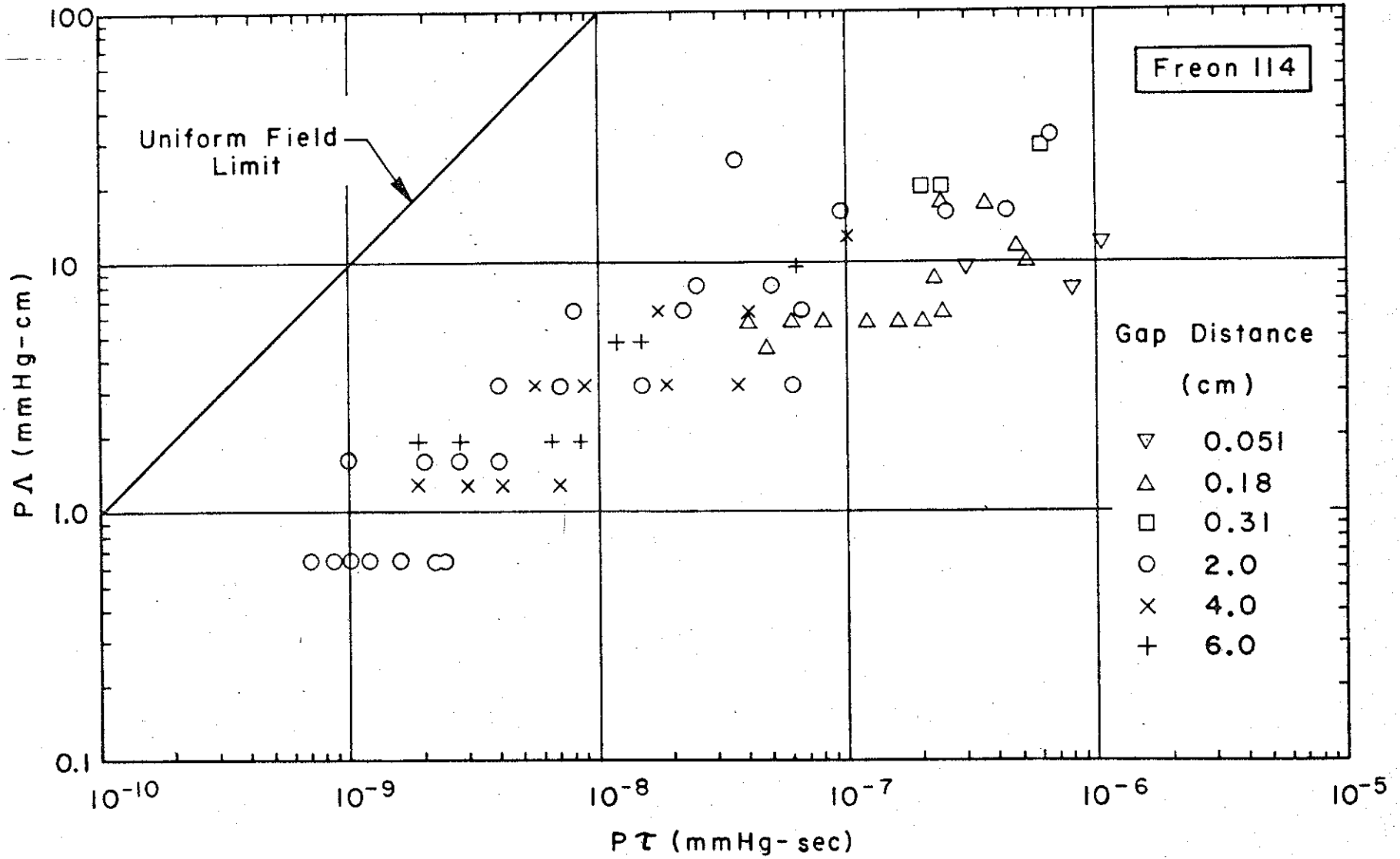

FIGURE 20.

FREON 114 EXPERIMENTAL DATA IN RELATION TO THEORY LIMITS.

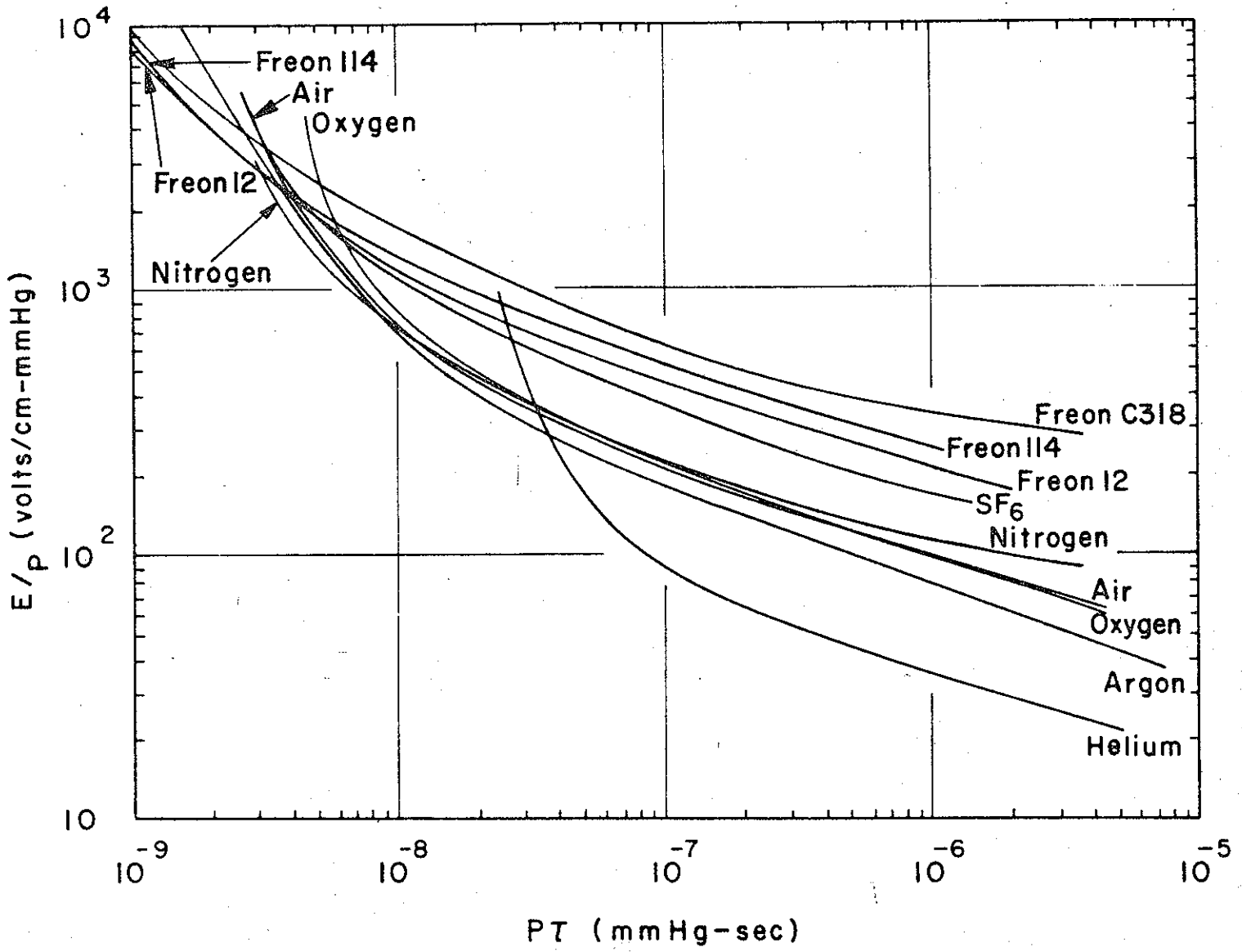

FIGURE 21.

BREAKDOWN CURVES FOR NINE TEST GASES.

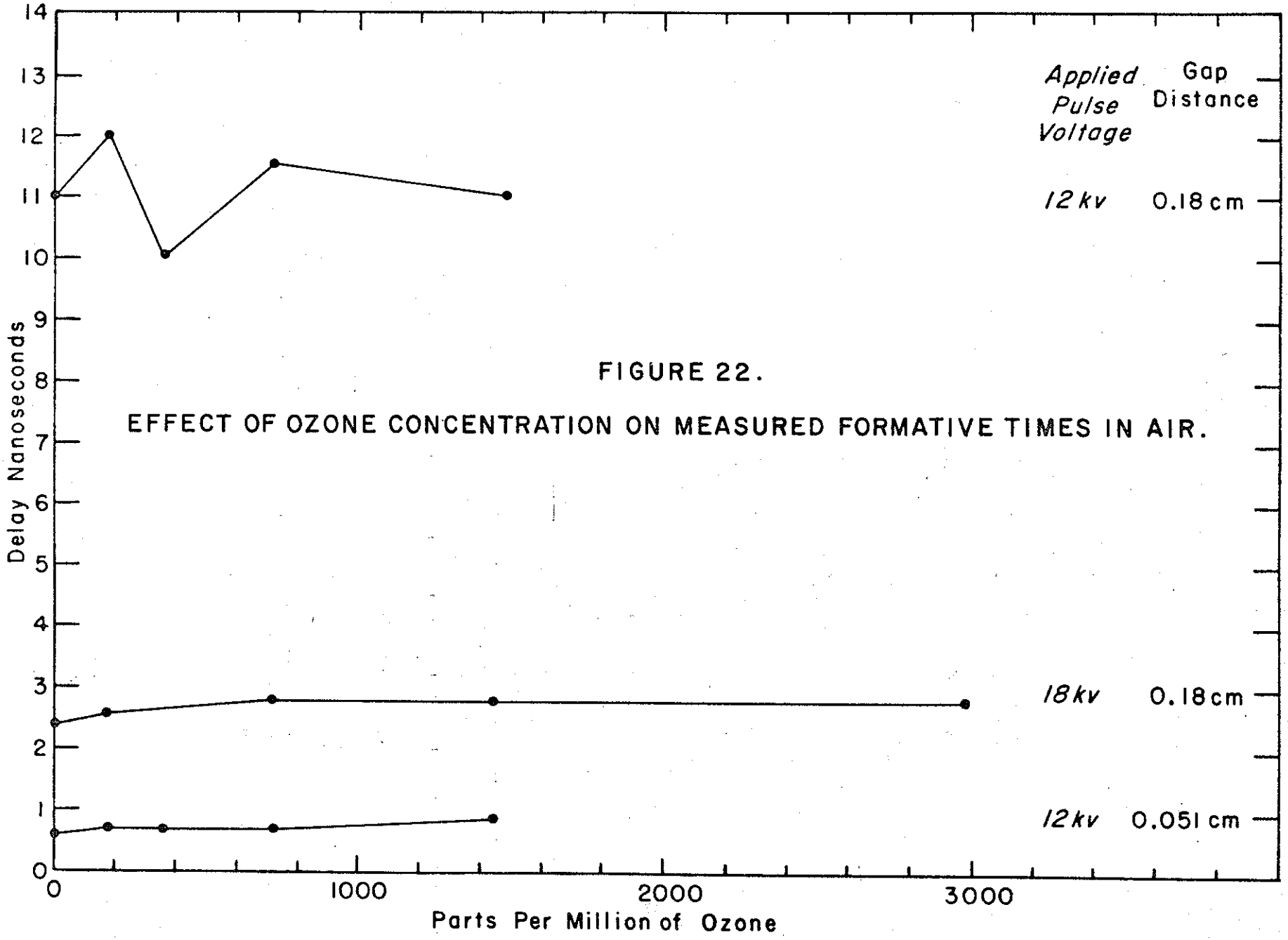

FIGURE 22.

EFFECT OF OZONE CONCENTRATION ON MEASURED FORMATIVE TIMES IN AIR.

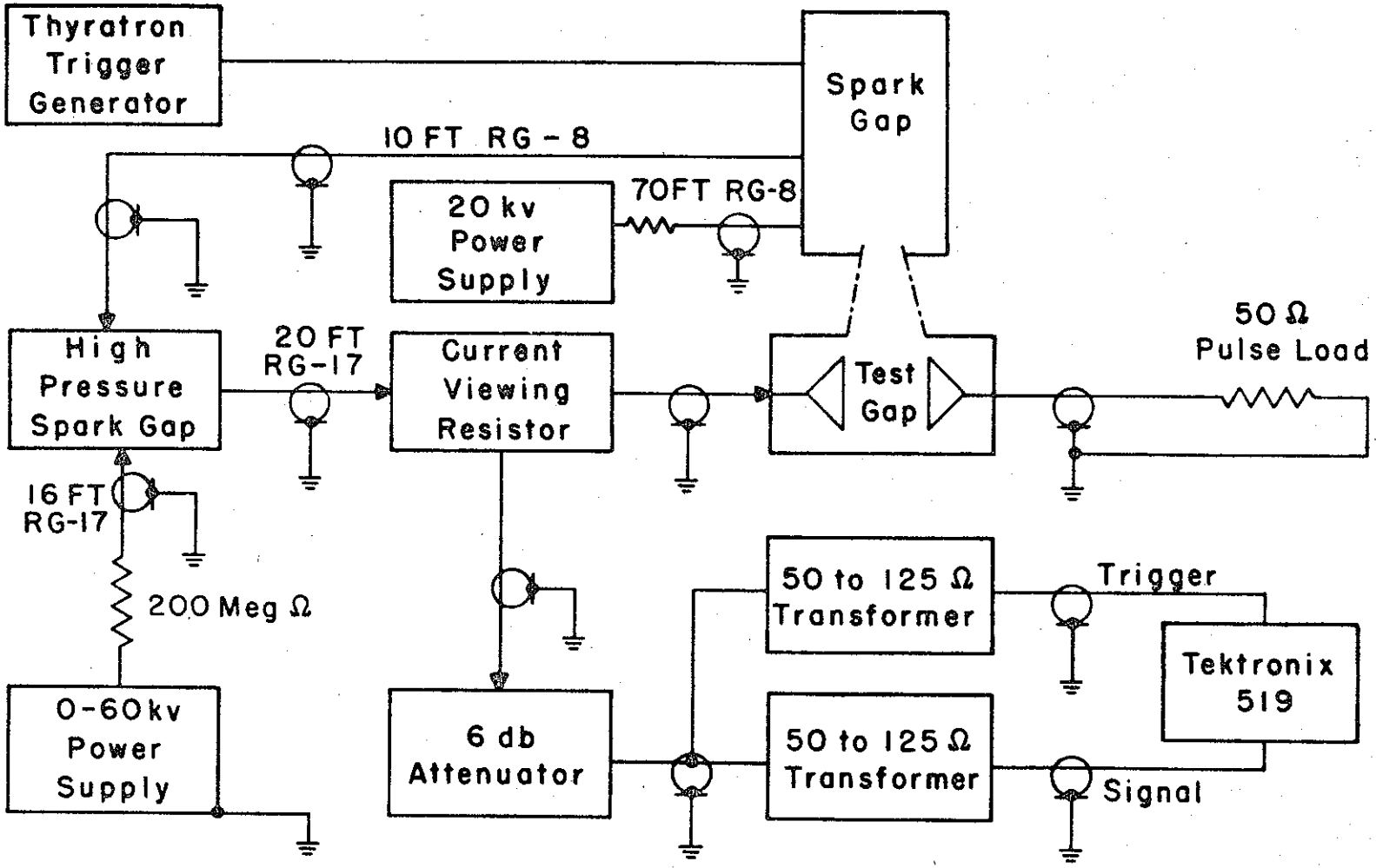

FIGURE 23.

SCHEMATIC DIAGRAM OF EXPERIMENTAL APPARATUS.

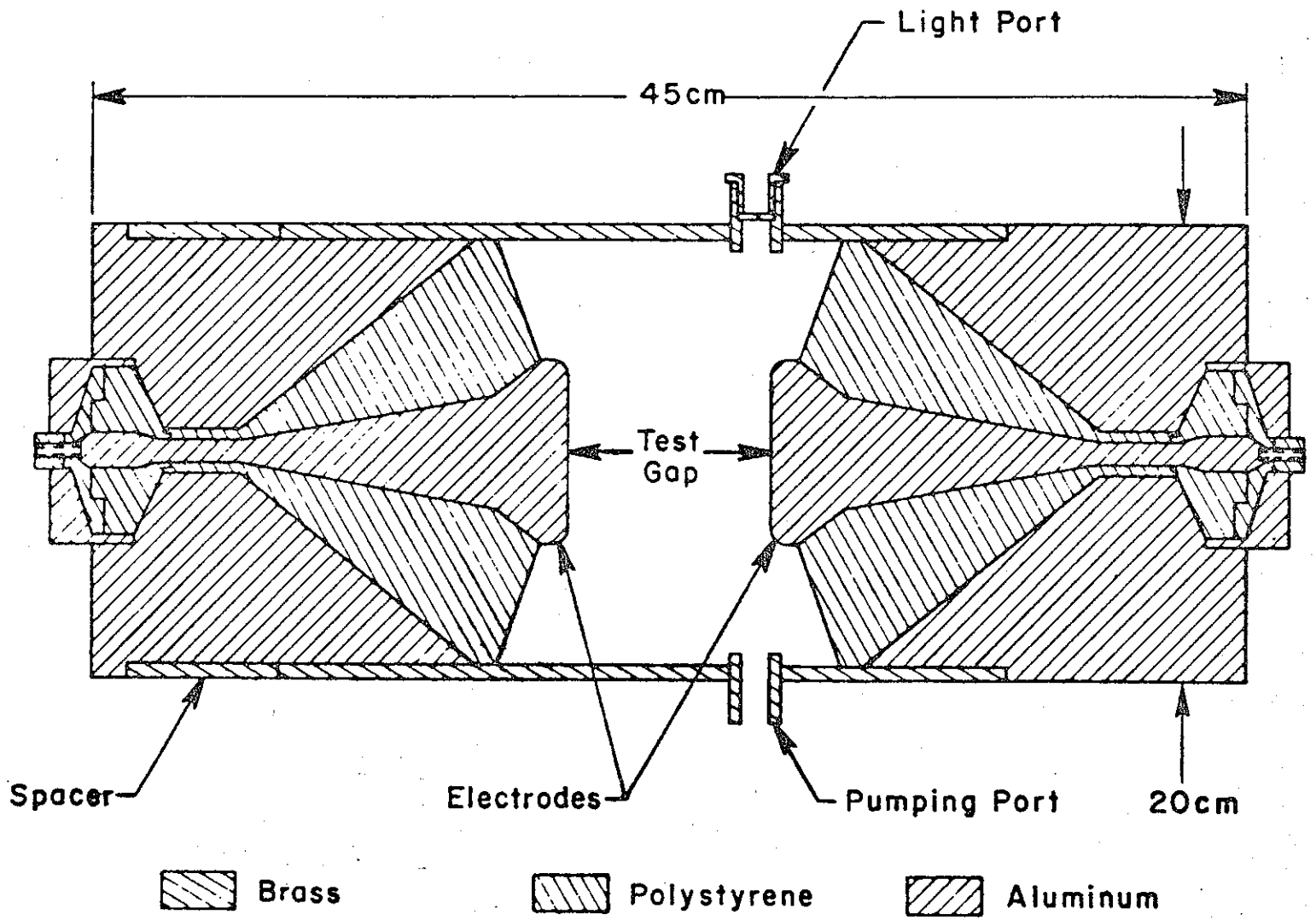

FIGURE 24.

CROSS SECTION OF LARGE TEST GAP.

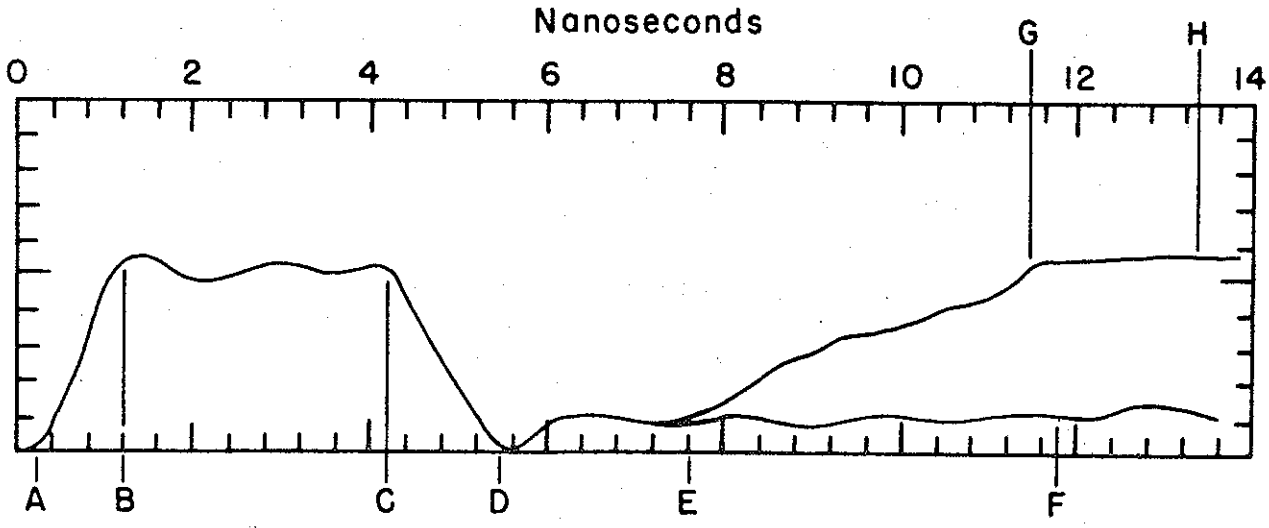

13 Kilovolts 4cm gap 5mmHg Air

FIGURE 25.

TYPICAL VOLTAGE WAVEFORM

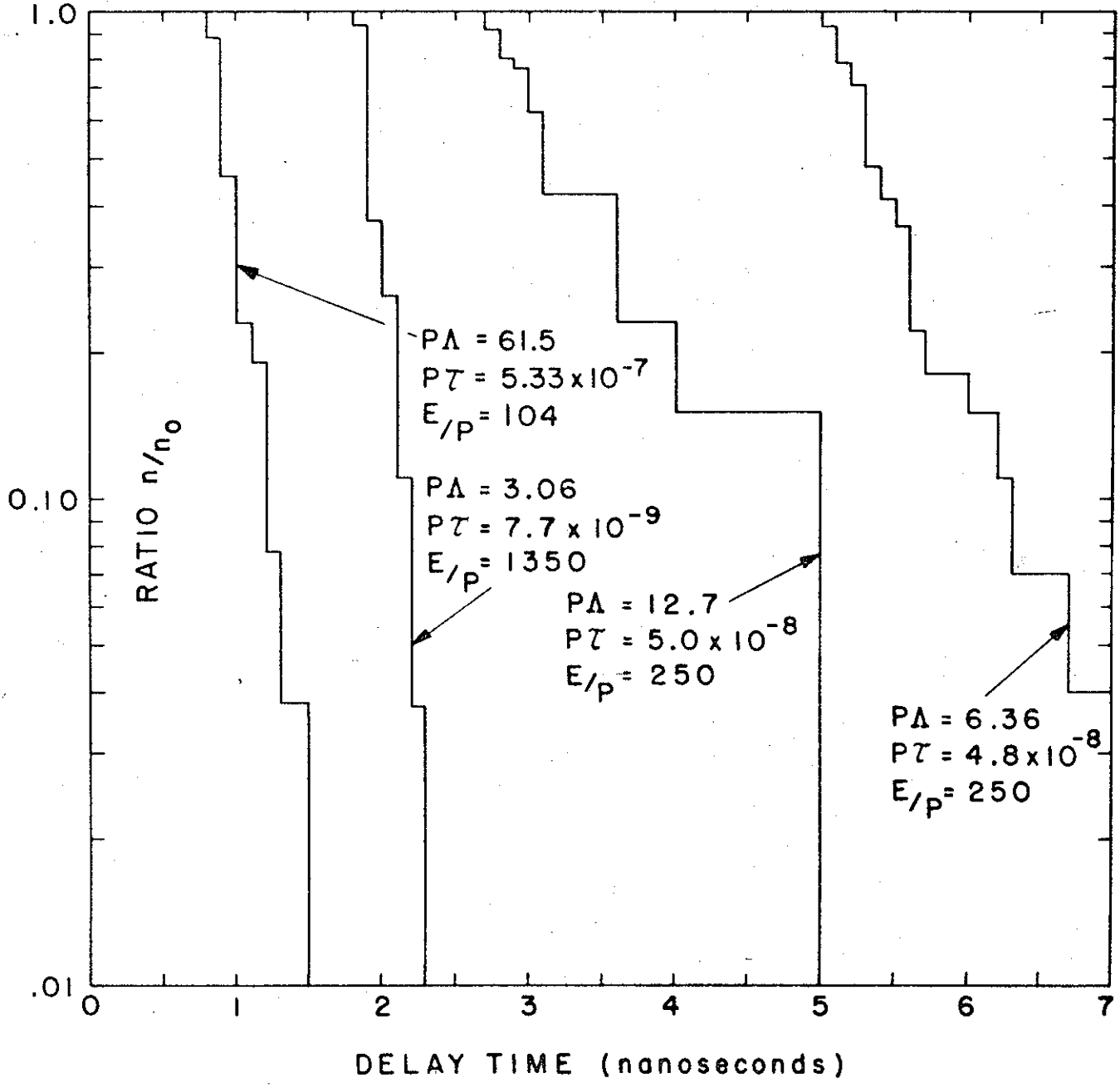

FIGURE 26.

LAUE PLOT OF STATISTICAL LAG FOR AIR.

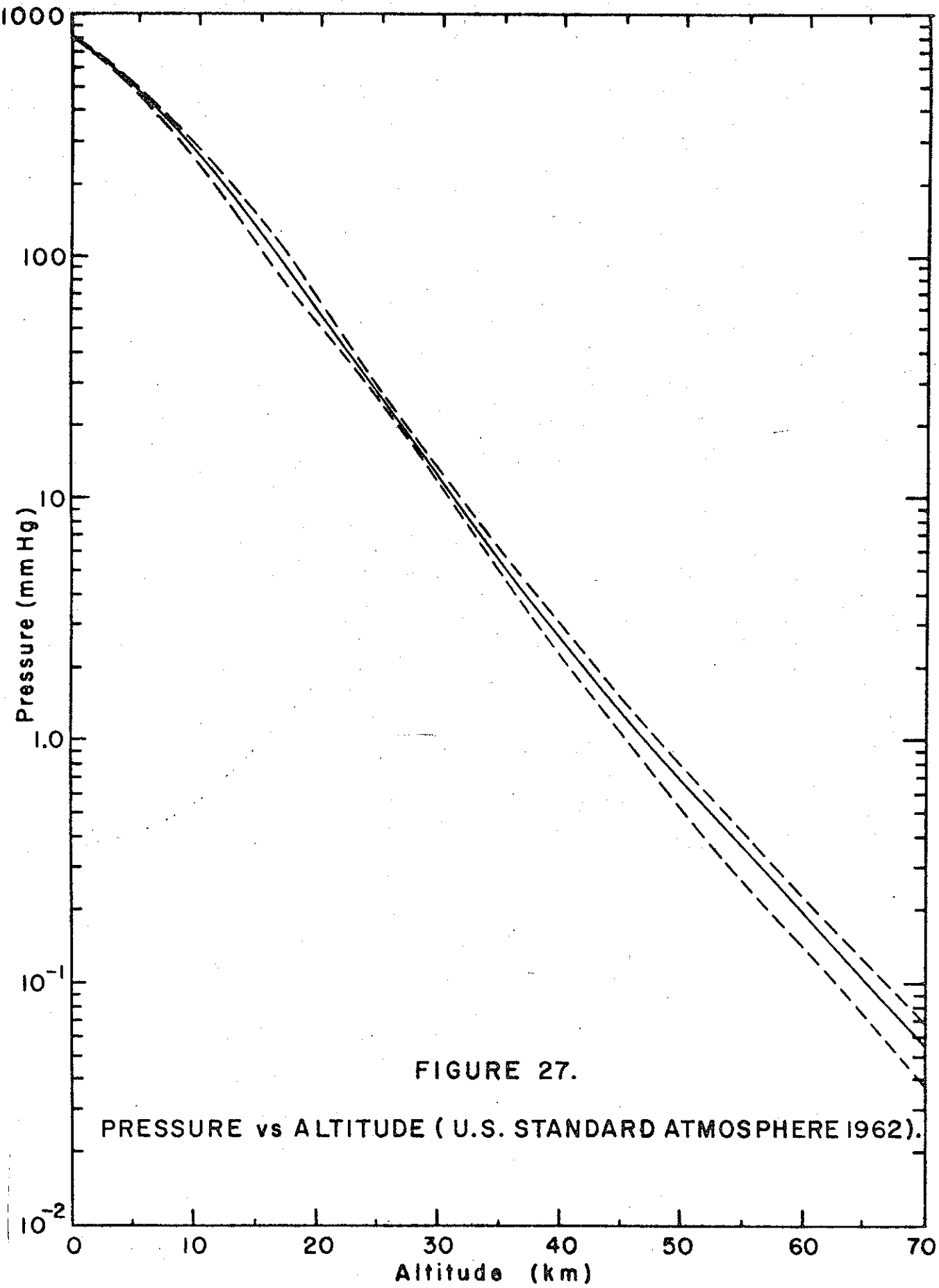

FIGURE 27.

PRESSURE vs ALTITUDE (U.S. STANDARD ATMOSPHERE 1962).

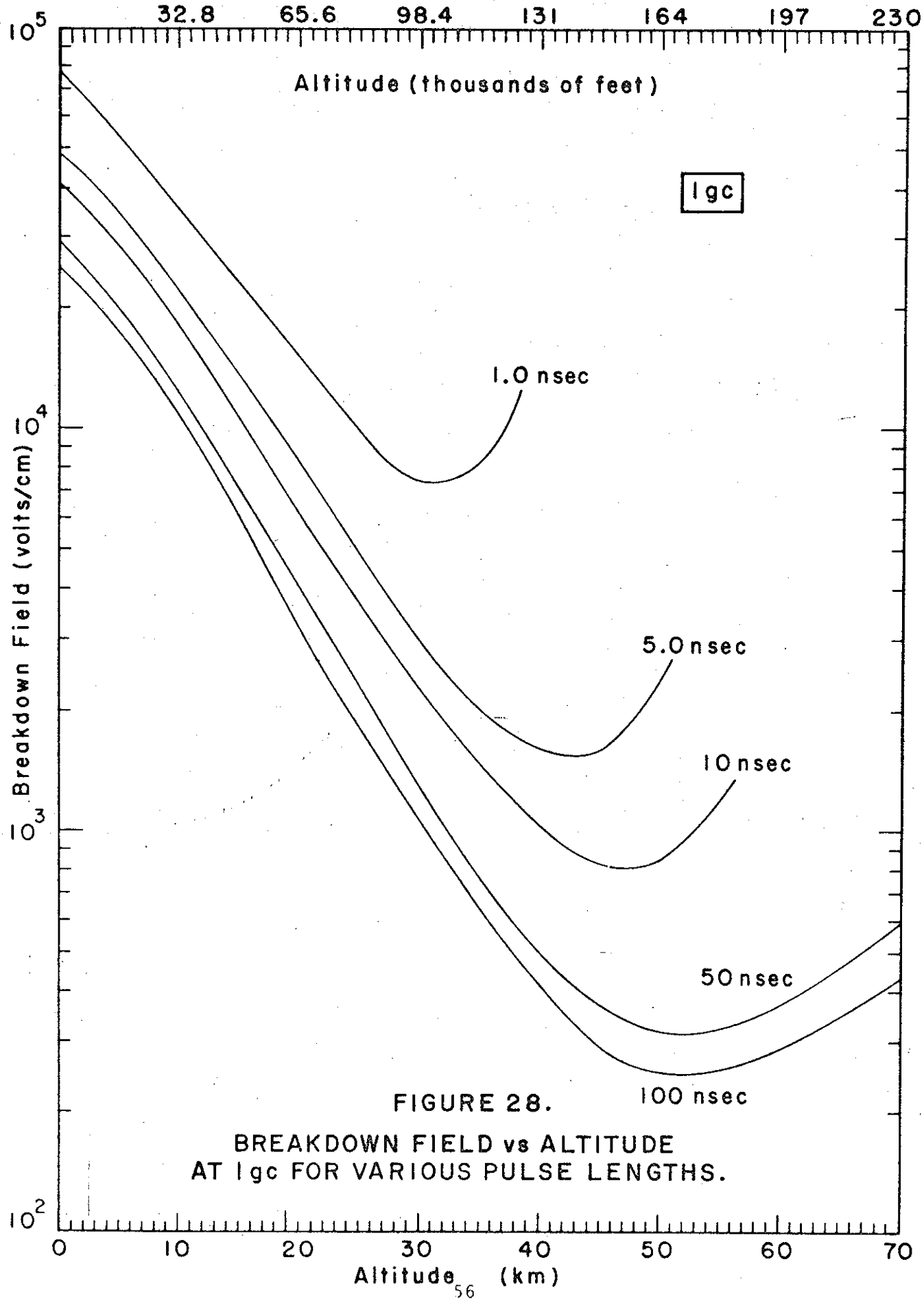

FIGURE 28.

BREAKDOWN FIELD vs ALTITUDE
AT 1gc FOR VARIOUS PULSE LENGTHS.

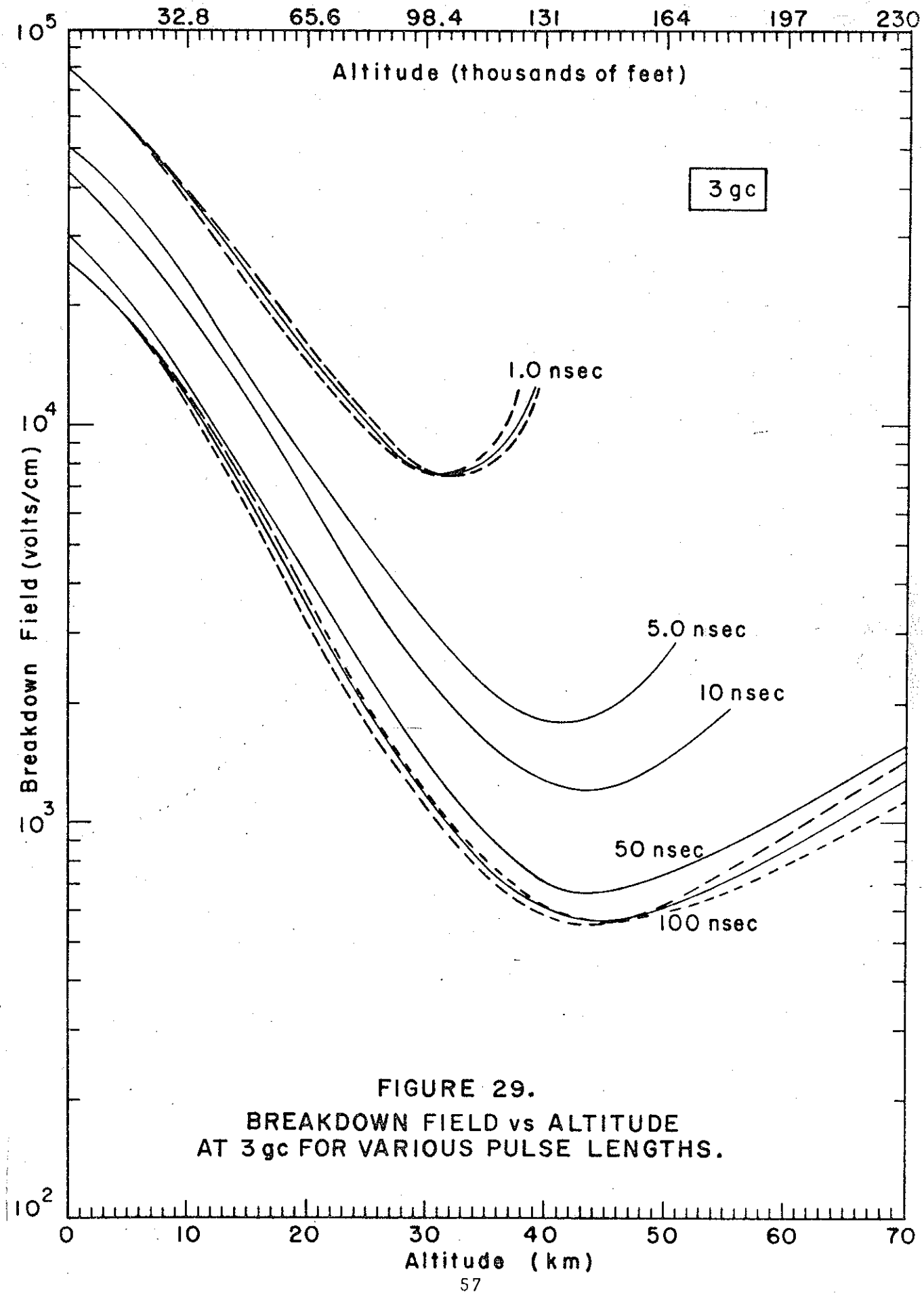

FIGURE 29.
BREAKDOWN FIELD vs ALTITUDE
AT 3 gc FOR VARIOUS PULSE LENGTHS.

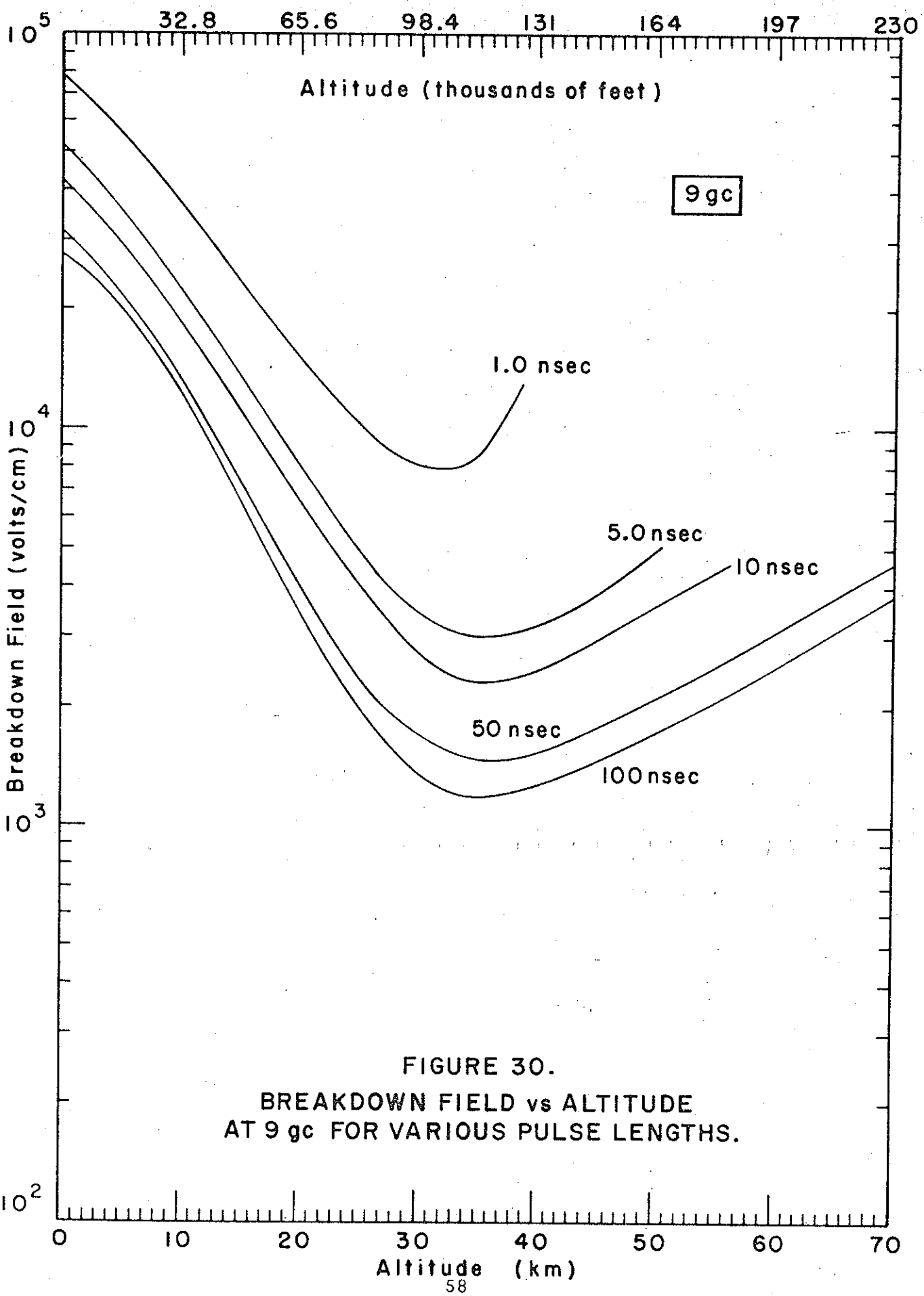

FIGURE 30.
BREAKDOWN FIELD vs ALTITUDE
AT 9 gc FOR VARIOUS PULSE LENGTHS.

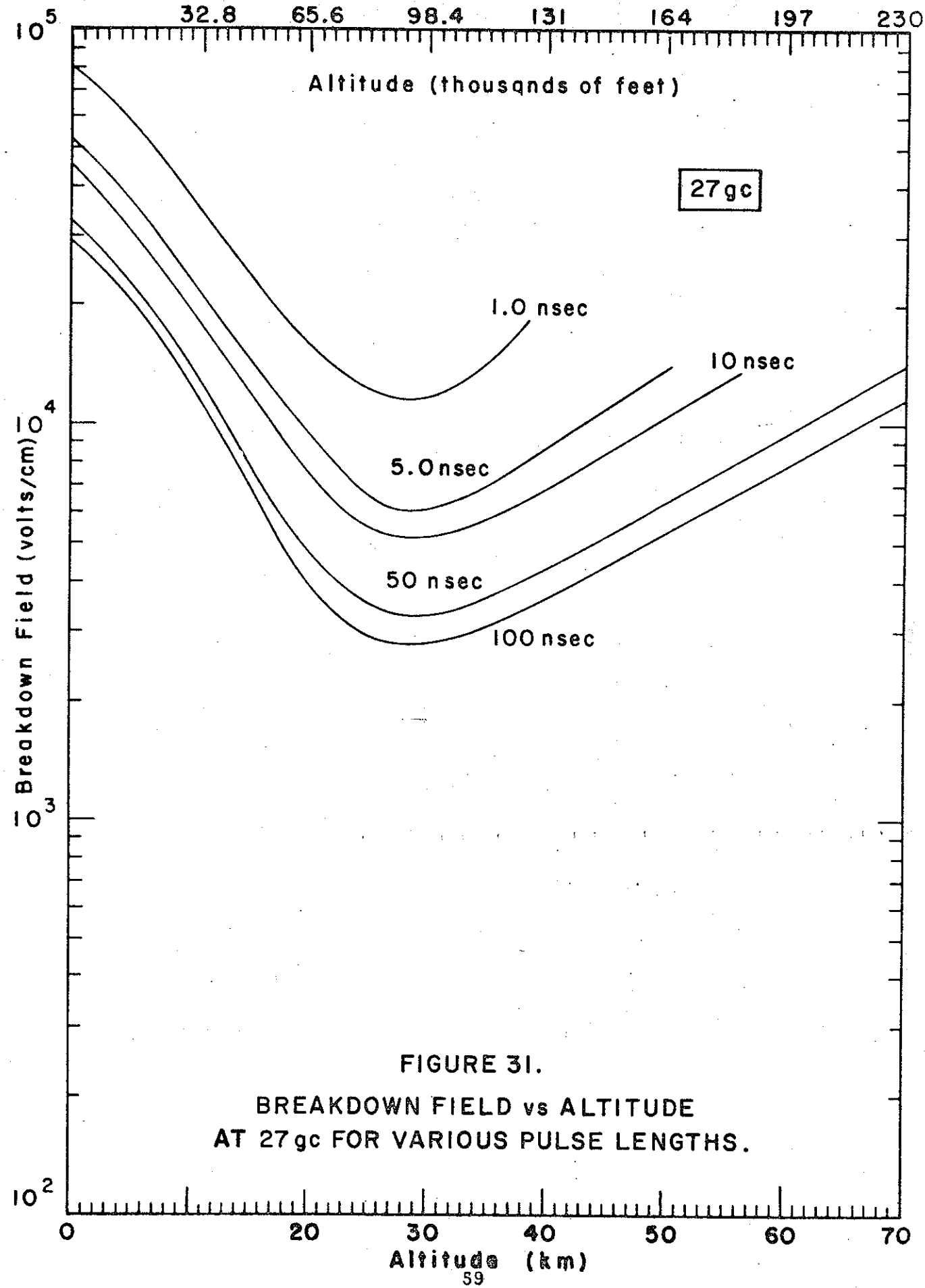

FIGURE 31.

BREAKDOWN FIELD vs ALTITUDE
AT 27 gc FOR VARIOUS PULSE LENGTHS.

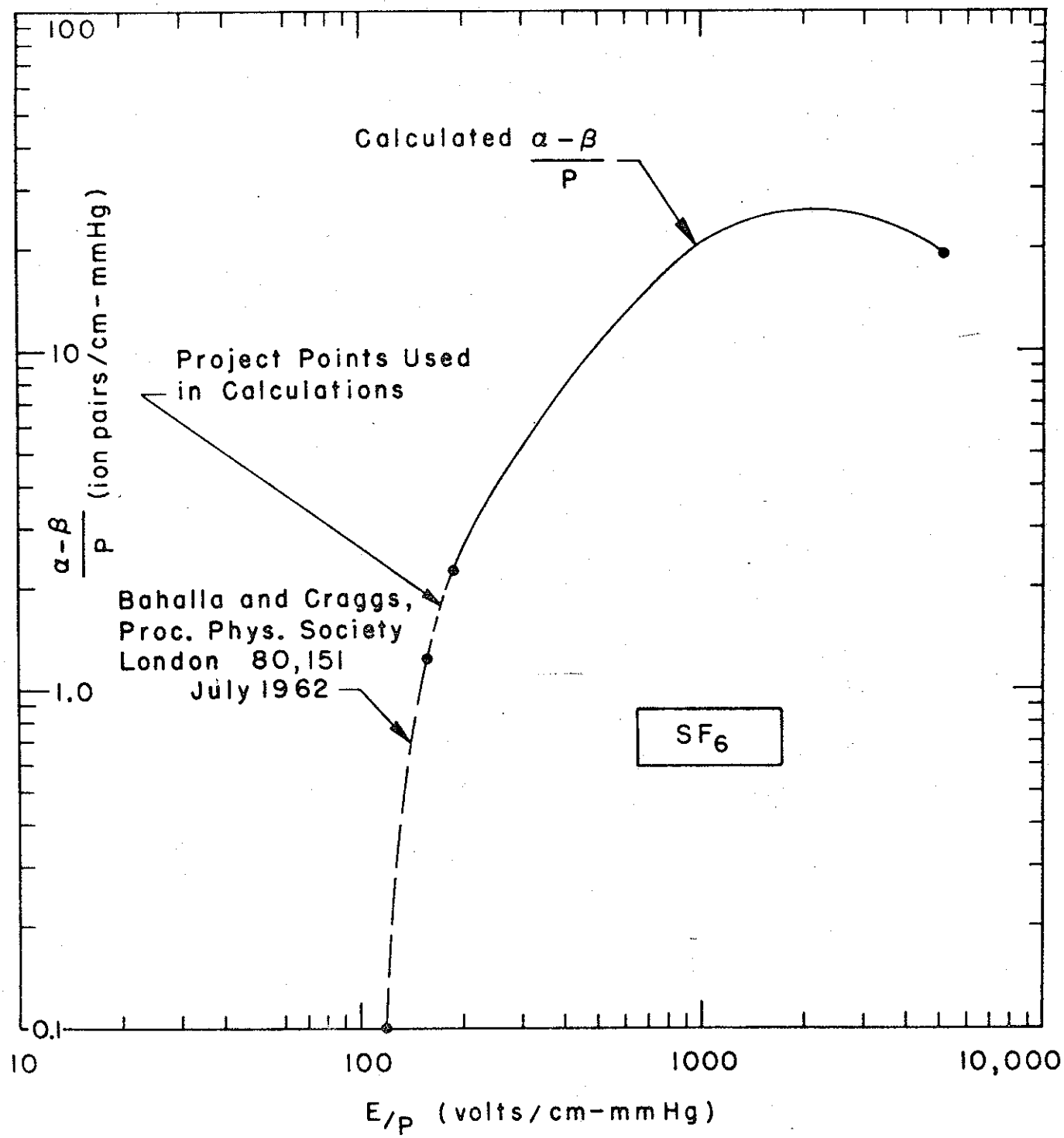

FIGURE 32.

THEORETICAL $\frac{\alpha-\beta}{P}$ CURVE FOR SULPHUR HEXAFLUORIDE.

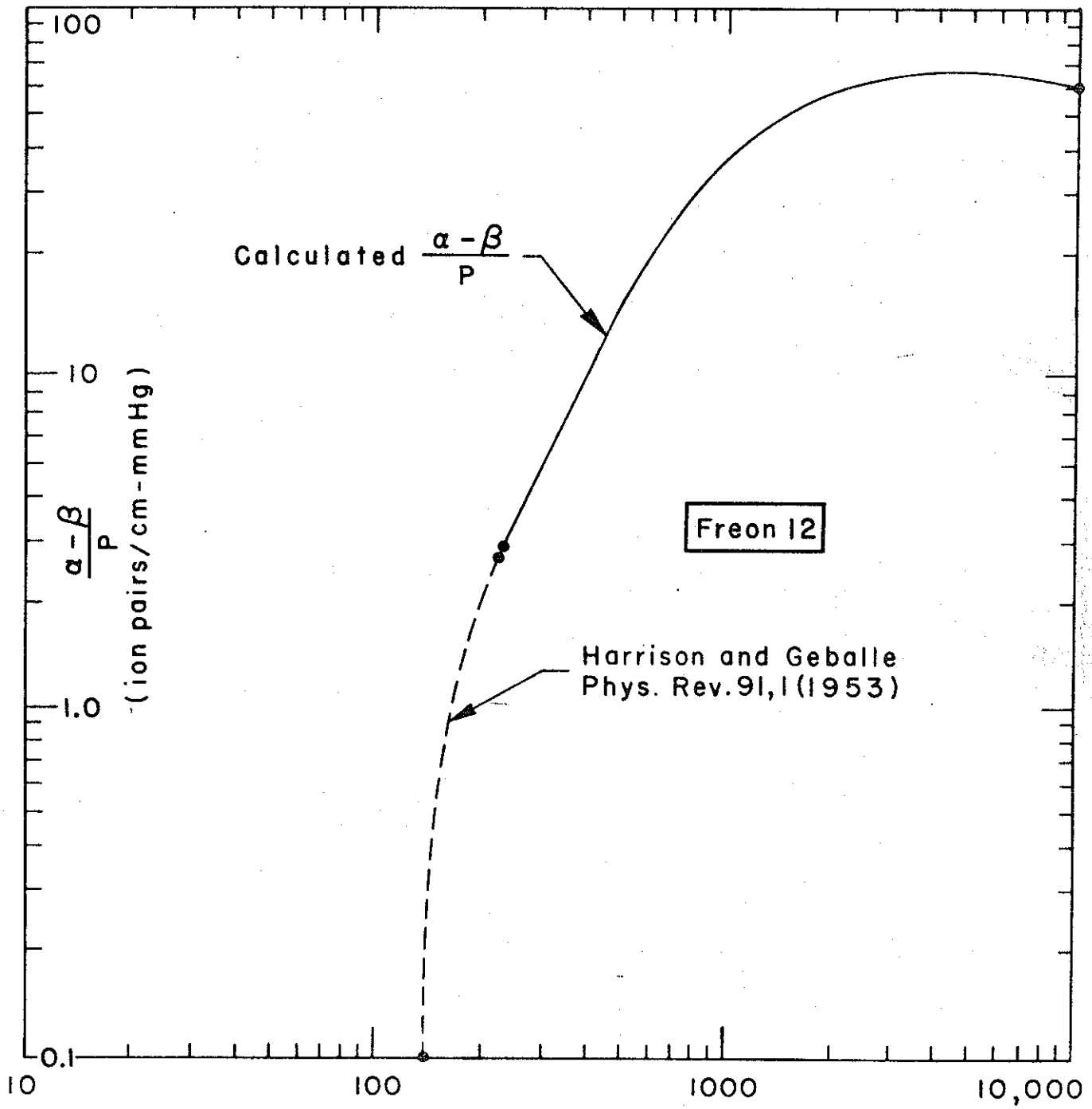

FIGURE 33.

THEORETICAL $\frac{\alpha-\beta}{P}$ CURVE FOR FREON 12.